UWB Radio-over-Fiber System Using Direct Modulated VCSEL

by

Su Li

A thesis
presented to the University of Waterloo
in fulfillment of the
thesis requirement for the degree of
Master of Applied Science
in
Electrical and Computer Engineering

Waterloo, Ontario, Canada, 2007

AUTHOR'S DECLARATION

I hereby declare that I am the sole author of this thesis. This is a true copy of the thesis, including any required final revisions, as accepted by my examiners.

I understand that my thesis may be made electronically available to the public.

Abstract

The demand for efficient and cost-effective transmission and distribution of RF signal is increasing with the rapid development of wireless communication. This thesis studies the effect of using cost-effective vertical cavity surface emitting laser (VCSEL) to distribute ultra wide band (UWB) RF signal. Properties of multimode and single mode VCSEL are studied and simulated using commercial optical design suite. One of the biggest drawbacks of Orthogonal Frequency Division Multiplexing (OFDM) used by UWB is high peak to average power ratio (PAPR). Signal pre-distortion method is proposed to mitigate nonlinear effect from VCSEL optical system. Software connector is implemented to interconnect the Optical and Wireless design suite. Integrated VCSEL optical link and UWB simulation is carried out for the performance of the radio-on-fiber (RoF) system. The RoF system with optimized single mode VCSEL and proposed pre-distortion method is found to be capable of distributing UWB RF signal.

Acknowledgements

I would like to thank Dr. Safieddin Safavi-Naeini, for his supervision in this study. I would also like to thank my thesis readers Dr. S. Hamidreza Jamali, Dr. A. Hamed Majedi and Dr. Xie Liang-liang for their support and feedback.

Dedication

To my father Xuanmin Li, my mother Minglan Chen, my wife Chunhua Zhao and my new born son Aaron Li, for their support and encouragement.

Table of Contents

List of Figures

List of Tables

Chapter 1 Introduction

Ultra wideband (UWB) communications is a fast emerging technology that offers new opportunities. UWB systems incorporating with time-hopping spread spectrum multiple access systems are one of the most promising technologies for short range high-throughput wireless communications. Current interests in UWB are fueled by their intrinsic properties: immunity to multi-path fading, extremely short time duration, low duty cycle, wide occupied bandwidth, and low power spectral density. UWB signals have important characteristics: huge bandwidth (0.5 to 10.6 GHz) and very low intensity, comparable to the level of parasitic emissions in a typical indoor environment (FCC part 15: -41.3 dBm/MHz). The ultimate target of UWB systems is to utilize broadband unlicensed spectrum (FCC: part 15: 3.1-10.6 GHz) by emitting noise-like signals. Low complexity and low power consumption of UWB technology is suitable for broadband services in the mass markets of wireless personal area networks (WPAN). UWB combines the high data rates with capabilities of localization and tracking features. Potential applications of UWB are wireless communications, intelligent transport system (ITS), imaging and sensors.

However, derived from the constraints on allowed emission levels and fundamental limits of thermal noise and Shannon limits [2] high data rate, UWB systems (e.g. 480 Mbps) are limited to short-ranges of less than 10m because of the emission requirement. While broadband access technology demands for larger coverage of high data rate UWB (10 – 10000 meters).

The UWB radio over optical fiber technology (UWB RoF) is a novel technology for the transmission of UWB signals by using an optical carrier propagating through an optical fiber. In this approach, the UWB RF signal itself is superimposed on the optical CW carrier. This strategy makes the conversion process transparent to the UWB's modulation method, and also transparency feature allows avoiding the high costs of additional electronic components required for synchronization and other processes.. The development of RoF systems is motivated by the demand for replacing a central high power antenna with a low power distributed antennas system (DAS). RoF systems are usually composed of many base stations (BSs), which are connected to

a single central station (CS). Therefore, many efforts have already been devoted to reduce the BS' cost and move the complexity to the CS.

Similar to conventional RoF, UWB RoF allows separation of low cost BSs from the CS. In conventional ROF, which targets the 2G/3G cellular systems, the RF signal bandwidth is only few 10's of MHz and its average power is in the range of several 100mW. This requires high cost photonic components in the CS and medium cost components in the BS. UWB RoF, on the other hand, is targeting the PAN market that is characterized by very low cost and low power (10's μ W) access point. In UWB RoF, the optical fiber is used to carry extremely wide RF signals (several GHz). There are other means to extend the short-range nature of the high data rate UWB system. But they are either practically not realizable due to link budget considerations or too expensive for the WPAN market. Over 10km length, the free space optical link approach suffers a 41 dB loss, roughly the same as 0.375 inch coax cable operating at 10 GHz [26]. In the free-space RF approach, the signal link losses at 4GHz center frequency would be more than 125dB over 10 km length. Compared to the extremely low loss level of optical fibers, the signal link losses is about 3dB at wavelength 1.55 μm over 10 km. 1Gbit/s Ethernet is a legacy approach to demodulate the UWB signal and transmit it digitally over single mode fiber. It is too expensive for WPAN applications. Furthermore, this solution is tailored to the specific UWB technology being employed. However UWB over fiber is much more generic and scalable solutions that can be easily applied to other less demanding cases, for example, range extension of wireless local area networks, WLAN. Solutions using ad-hoc and multi-hop network topologies to deliver the high data rate between the nodes of WPAN would lead to greater network delays.

In this study, pre-distortion method for UWB signal is proposed; limitations are identified to optimize RoF system. With the proposed pre-distortion method and optimized single mode VCSEL, for 500m optical link, SFDR of 80 – 90 dB $Hz^{2/3}$, the RoF system achieved the performance of 1.54302e-4 for the BER at SNR 30 dB. The low cost RoF system with optimized single mode VCSEL and pre-distortion method is found to satisfy the requirements to distribute UWB RF signal.

Chapter 2 Radio-over-Fiber Technologies

Radio over Fiber (RoF) is an optical fiber link to distribute modulated RF signals from a central location to remote antenna units (RAUs). The RoF systems are developed to replace a central antenna with a low power distributed antennas system (DAS) [3]. RoF systems are usually composed of many base stations (BSs), which are connected to a single central station (CS) (See Figure 2-1). RoF systems centralize the RF signal processing function in one shared location (headend), and use optical fiber link to distribute the RF signals to the RAUs or BSs. RoF based wireless "last mile" access network architecture was proposed [5], as a promising alternative to broadband wireless access network. In network archietecure, the CS performs all switching, routing and network operations administration maintenance (OAM). Optical fiber network interconnects a number of simple and compact antenna BSs for wireless distribution. The BS has no processing function and the main function of the BS is to convert the optical signal to wireless and vice versa. This architecture assumes a centralized medium access control (MAC) located at the CS responsible for offering a reservation-based, collision-free medium access.

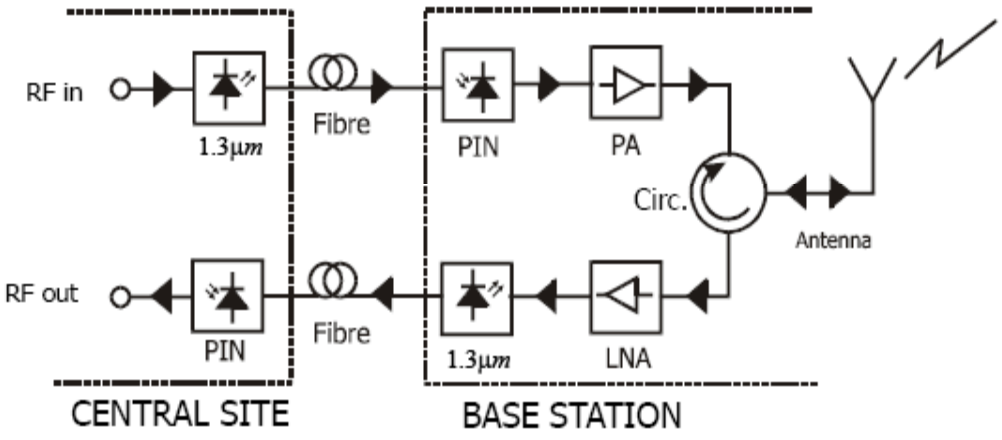

Figure 2-1 Radio on Fiber System [3]

2.1 Application of Radio on Fiber

The main application areas are briefly introduced as the following:

1) Cellular Networks
   Mobile traffic (e.g. CDMA, GSM, UMTS) can be relayed cost effectively between SCs and BSs via RoF system. RoF can also be applied to radio coverage extension in dense urban environments and capacity distribution and allocation [6].
2) Wireless LANs
   The demand for mobile broadband access to LANs increases as mobile devices become more popular. RoF can be applied to distribute Wireless LANs signals operating at 2.4 GHz and 5 GHz. This leads to more efficient base station design for micro and pico cell.
3) Video Distribution Systems
   RoF for metropolitan area networks (MAN), both wired (Cable TV) and wireless (IEEE 802.16x) broadband access systems.
4) Vehicle Communication and Control
   Rof can be used in Intelligent Transport Systems (ITS), road-to-vehicle communication systems using, e.g. the 36/37 GHz carrier frequency [6]. Frequencies between 63-64 GHz and 76-77 GHz have been allocated for ITS in Europe. RoF extends the coverage of the road network and makes ITS more manageable and effective.

Fiber optical links that support transmission of entire RF band of few GHz over large distance are of a great importance. Compared to the wireless or wired-coax channel, the fiber link losses are very small. The power budget of a UWB RoF system is determined by the contributions of RF losses, optical fiber losses and conversion losses. RF-optical conversion losses dominate the power budget. The total losses can be substantially reduced by using optical fibers instead of a cable or wireless transmission due to the extremely low losses per unit length of an optical fiber. Development of efficient and cost-effective RF-optical links for UWB technology is a main objective of our research.

2.2 Advantages of RoF Systems

Some of the advantages and benefits of the RoF distribution are discussed below.

1) High Bandwidth

Optical fibers have three main transmission windows, which offer low attenuation for optical fiber: 850 nm, 1310 nm, and 1550 nm wavelengths. The combined bandwidth of the three windows for single mode fiber is more than 50 THz [10]. The commercial optical system only utilizes a fraction of the capacity (about 1.6 THz). High bandwidth means high transmitting capacity. Some signal processing that may be difficult or impossible to do in electronic system be resolved by the high bandwidth of optical system. For example, some of the demanding microwave functions such as filtering, mixing, up and down conversion, can be implemented in the optical domain [11].

2) Low Attenuation

Optical fiber has very low loss. RoF technology can be used to achieve both low loss distribution of RF signal, and simplification of RAUs at the same time. Single mode fibers (SMFs) made from silica have attenuation losses below 0.2 dB/km and 0.5 dB/km in the 1550 nm and the 1300 nm windows, respectively. Polymer Optical Fibers (POFs) has attenuation ranging from 10 to 40 dB/km in the 500-1300 nm range [9]. These losses are much lower than the losses for coaxial cable, whose losses are higher by three orders of magnitude at higher frequencies. Comparing to electrical distribution of RF signal either in free space or transmission lines, by transmitting RF in the optical form, transmission distances are increased several times and the required transmission powers are greatly reduced.

3) Immunity to Radio Frequency Interference

Optical fiber has immunity to electro-magnetic interference (EMI). This is because signals are transmitted in the form of light in the optical fiber. Immunity to eavesdropping is another important characteristic of optical fiber. This provides privacy and security.

4) Low Power Consumption

Simple RAUs with reduced equipment leads low power consumption. Most of the complex equipment is kept at the centralized head end. Some applications, the RAUs are even operated in passive mode. For some other applications, RAUs are sometimes placed in remote locations not fed by the power grid; power consumption reduced at the RAU is significant

5) Multi-Service Capable

RoF offers system operational flexibility using sub-carrier modulation (SCM). RoF transmission system can be made signal format transparent. For instance the Intensity Modulation and Direct Detection (IM-DD) technique can be made to operate as a linear system and therefore as a transparent system. This can be achieved by using low dispersion fiber in combination with SCM RF signals. In that case, the same RoF network can be used to distribute multi-operator and multi-service traffic. This brings in huge economic savings.

6) Dynamic Resource Allocation

In RoF system, switching, modulation, and other RF functions are performed at a centralized head-end. This makes it possible to allocate capacity dynamically. For instance, RoF system for cellular network, more capacity can be allocated to an area (e.g. downtown area) during peak times and then re-allocated to other areas when off-peak. Allocating capacity dynamically as need saves resources in cases where traffic loads vary frequently and by large margins. Having the centralized head-end can also consolidate other signal processing functions such as mobility functions, and macro diversity transmission [4].

2.3 Limitations of RoF Systems

Since RoF involves analogue modulation, and detection of light, it is fundamentally an analogue transmission system. Therefore, signal impairments such as noise and distortion, which are important in analogue communication systems, are important in RoF systems as well. These impairments tend to limit the Noise Figure (NF) and Dynamic Range of the RoF links. Dynamic Range is a very important parameter for wireless communication systems such as GSM and WLAN because the power received at the BS from the MUs varies widely (e.g. 80 dB [4]). That is, the RF power received from a MU, which is close to the BS, can be much higher than the RF power received from a MU, which is several kilometers away, but within the same cell.

The noise sources in analogue optical fiber links include the laser's Relative Intensity Noise (RIN), the laser's phase noise, the photodiode's shot noise, the amplifier's thermal noise. In Single Mode Fiber (SMF) based RoF, systems, chromatic dispersion may limit the fiber link

lengths and may also cause phase de-correlation leading to increased RF carrier phase noise [15]. In Multi-Mode Fiber based RoF systems, modal dispersion severely limits the available link bandwidth and distance. It must be stated that although the RoF transmission system itself is analogue, the radio system being distributed need not be analogue as well, but it may be digital (e.g. WLAN, UMTS), using comprehensive multi-level signal modulation formats such as xQAM, or Orthogonal Frequency Division Multiplexing (OFDM).

2.4 Up-conversion from RF to Optical Domain

Up-conversion from RF to Optical Domain can be realized either by direct laser modulation or external modulation methods [16]. Direct methods have the advantages of simplicity, low cost. Their main disadvantages are relatively limited bandwidth (10 GHz), high chirp, non-linear and inter-modal distortion, and SNR limited by Relative Intensity Noise (RIN). Common external modulation methods are:

a) Mach-Zehnder (MZ) interferometer having characterized by limited bandwidths (2-3 GHz), high linearity, low chirp, and high bias voltage. In particular, traveling wave (TW) configuration of the MZ modulator permits to overcome the bandwidth limitations.

b) Electroabsorption modulator (EAM) characterized by high bit rate, compatibility with the advanced photonic technologies. EAMs based on the quantum confined Stark effect (QCSE) in quantum wells can exhibit excellent performance.

Due to high performance combined with low manufacturing cost, the Vertical Cavity Surface Emitting Laser (VCSEL) has become an established light source in data communication networks such as Local Area Networks (LANs) and Storage Area Networks (SANs)) where the VCSEL is on-off modulated for the transmission of digital signals. With the rapid developments of wireless communication networks there is also an increasing demand for simple, power-efficient and cost-effective transmission and distribution of RF signals over optical fibers. One such example is Distributed Antenna Systems (DAS) for in-building coverage in cellular systems for mobile communication and wireless LANs (WLANs), operating in the 1-5 GHz range [4]. While VCSELs fulfil the performance requirements of on-off modulated digital links at bit rates

well in excess of 10 Gbit s^{-1} [17], it is not obvious that they also fulfil the requirements of analogue links operating in the GHz range, since such links are in some aspects more demanding. Laser characteristics of particular importance for analogue links are the impedance, modulation efficiency, linearity and intensity noise. These laser parameters often limit the dynamic range, the gain, and the noise figure of analogue fiber optic links [24].

Chapter 3 UWB Overview

Ultra Wideband (UWB) is expected to have a major impact on the wireless world vision of 4G systems. It is a fast emerging technology that offers new opportunities and the important characteristics of UWB signals are the following: huge bandwidth (0.5 to 10.6 GHz) and very weak intensity, comparable to the level of parasitic emissions in a typical indoor environment (FCC part 15: -41.3 dBm/MHz). The ultimate target of UWB systems is to utilize broadband unlicensed spectrum.

There are three main flavors of UWB technologies are proposed for PAN wireless communication. Impulse radio (IR-UWB), direct sequence (DS-UWB), and multi-band OFDM (MB-OFDM), see updated survey in [26]. In this thesis we focus on MB-OFDM UWB from IEEE P802.15 Working Group for Wireless Personal Area Networks (WPANs). MB-OFDM [28] is based on subdividing the UWB spectrum into 5 band groups and 14 sub-bands of 528MHz width (Figure 3-1). Only band group 1 is mandatory while 2 to 5 are optional. The UWB system provides a wireless PAN with data payload communication capabilities of 55, 80, 110, 160, 200, 320, and 480 Mb/s. The support of transmitting and receiving at data rates of 55, 110, and 200 Mb/s is mandatory. The proposed UWB system employs Orthogonal Frequency Division Multiplexing (OFDM). The system uses a total of 122 sub-carriers that are modulated using Quadrature Phase Shift Keying (QPSK). Forward error correction coding (convolutional coding) is used with a coding rate of 11/32, ½, 5/8, and ¾.

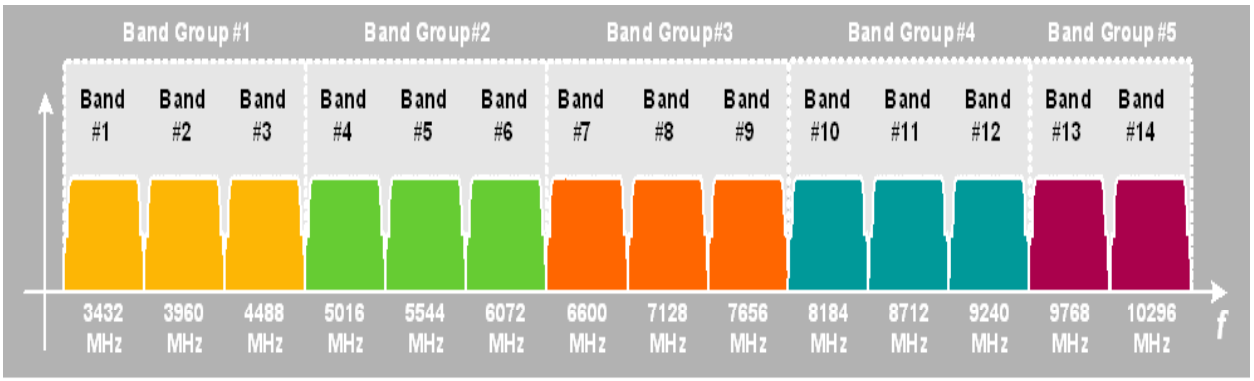

Figure 3-1 MB-OFDM Band Plan [26]

3.1 Time-Frequency Interleaving

The full-band time frequency interleaved OFDM system is similar to that of conventional OFDM except that only a contiguous subset of the tones are used for a single OFDM symbol. Between consecutive OFDM symbols, different subsets of tones are used. This is equivalent to coding the data in both time and frequency. Using the scheme of varying the subset of tones as a function of time (or OFDM symbol), the speed of DAC at the sender and ADC at the receiver is lowered. The same transmit power as a full-band signal (that occupies the complete bandwidth spanned by the IFFT) can be obtained using lower speed time frequency interleaved OFDM. UWB transmit architecture block diagram is shown in Figure 3-2. The structure of the transmitter is very similar to that of a conventional wireless OFDM physical layer, except that the carrier frequency is changed according to the interleaving kernel.

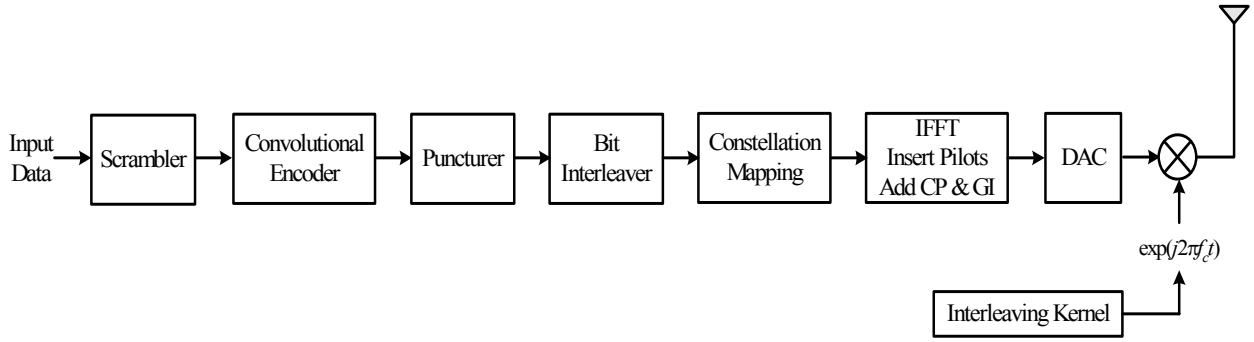

Figure 3-2 UWB Transmitter Architecture

A UWB system that uses a 512-point IFFT with a tone spacing of 4.125 MHz is shown in Figure 3-3. The UWB signal spans the entire bandwidth from 3168 MHz to 5280 MHz. UWB requires a minimum bandwidth if 500 MHz. However we do not need to transmit on all tones to be a compliant UWB system. As a mater of fact, transmitting only 122 tones to generate a signal that has a bandwidth greater than 500 MHz meets the UWB requirement. To simplify the implementation, we can first work on only subsets that contain a total of 128 consecutive tones. Therefore, the 512-point IFFT can be divided into 4 non-overlapping sets of 128 tones. Only 128 tones are used to generate a single OFDM symbol. To reduce the system complexity, the 512-point IFFT can be replaced with128-point IFFT.

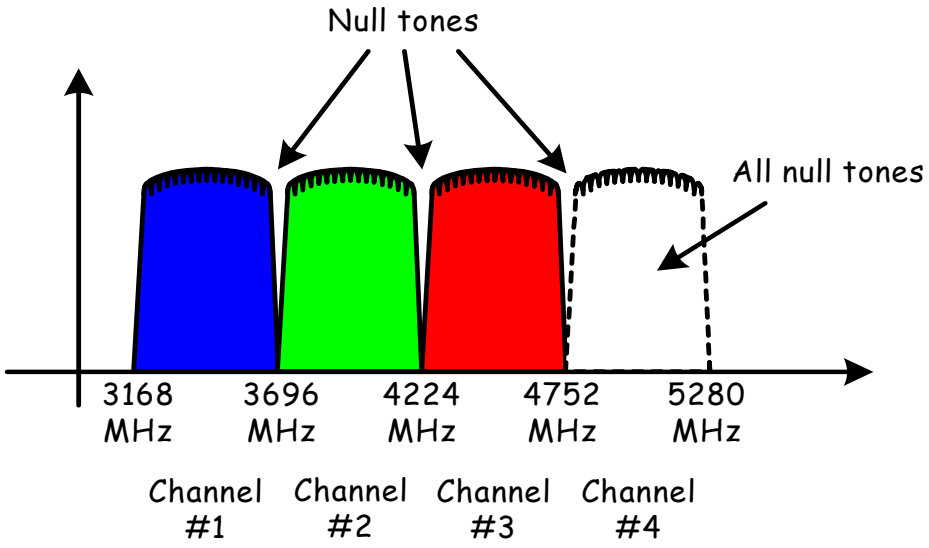

Figure 3-3 An Example of A Multi Carrier OFDM System [28]

Figure 3-4 shows an example of how the data is transmitted on different subsets of tones. In this example, data is transmitted in OFDM symbol #1 on the first 128 tones (tones 1 through 128). For OFDM symbol #2, data is transmitted on tones 257 through 384 (third set of tones). For OFDM symbol #3, the data is transmitted on tones 129 through 256 (second set of tones). For OFDM symbol #4, the data is transmitted on the first 128 tones (tones 1 through 128), and so on. It can be generalized that the period for this time-frequency coding pattern is three.

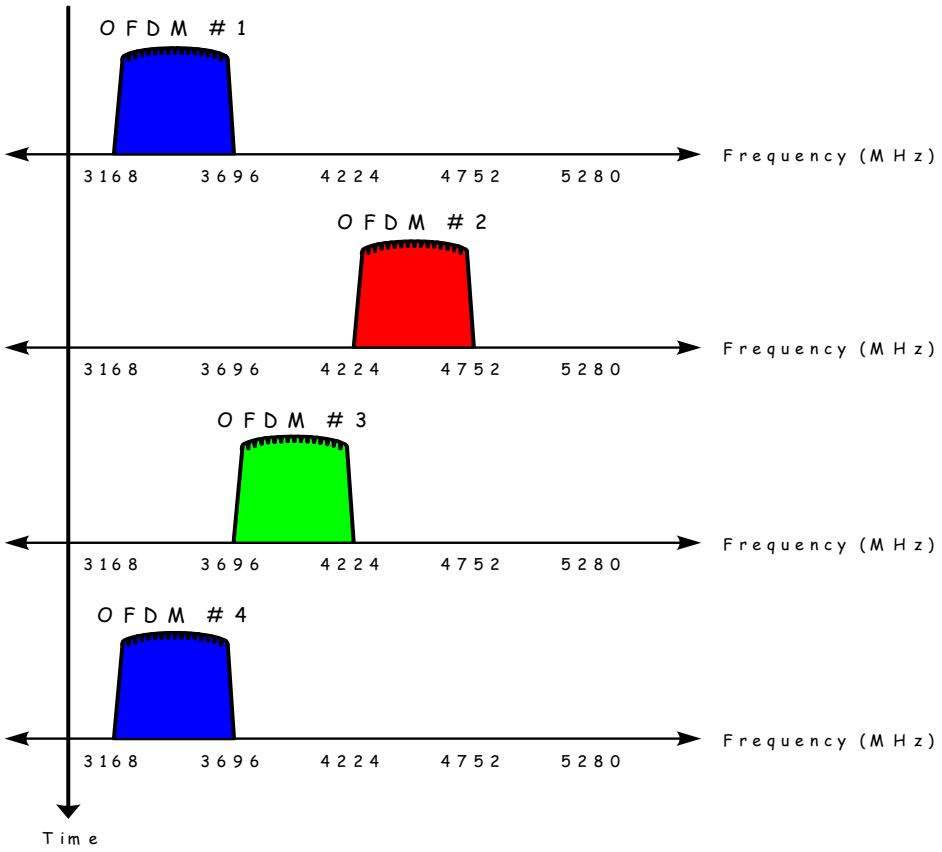

Figure 3-4 Frequency Domain Representation for Time Frequency Interleaving OFDM As A Full-band System [28]

Figure 3-5 shows an alternative view of the time-frequency coding of Time Frequency Interleaving OFDM in the time-domain, where the OFDM symbols are interleaved across both time and frequency. From Figure 3-5 we can see, the first OFDM symbol is transmitted on channel #1, the second OFDM symbol is transmitted on channel #3, the third OFDM symbol is transmitted on channel #2, the fourth OFDM symbol is transmitted on channel #1, and so on. We have implicitly assumed that the time-frequency interleaving is performed across three OFDM symbols. But in practice, the interleaving period can be much longer. The exact length and pattern of the time-frequency interleaving may differ from superframe to superframe and piconet to piconet.

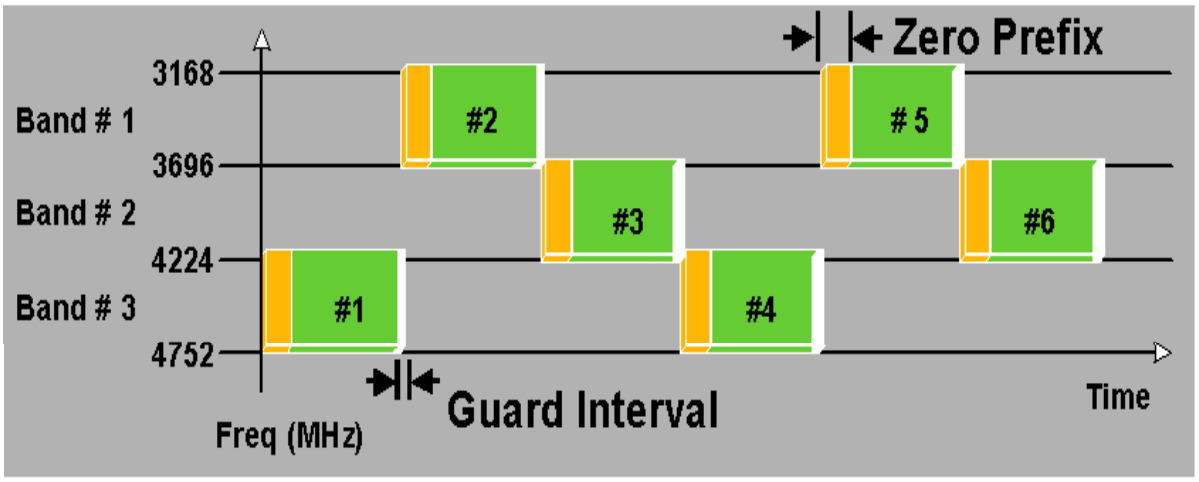

Figure 3-5 An Example of The Time-Frequency Interleaving Used in the Proposed UWB [28]

From Figure 3-5, we also see that a guard interval is inserted after each OFDM symbol. By inserting the guard interval between OFDM symbols, the complexity of the transmitter can be reduced. Instead of using a 512-point IFFT and a single carrier frequency, we can implement the same system using a 128-point IFFT and variable carrier frequencies. The reason that we can use a 128-point IFFT is that data is transmitted only on 128 of the 512 tones that are available at the IFFT. The guard interval is included to ensure that the transmitter and receiver have sufficient time to switch from the current channel to the next channel. Thus, the Time Frequency Interleaving OFDM system can be viewed as both a full-band UWB system and as a sub-band UWB system.

3.2 UWB Signal Mathematical Description

The transmitted signals can be described using a complex baseband signal notation. The actual RF transmitted signal is related to the complex baseband signal as follows [28]:

$$r_{RF}(t) = \mathrm{Re}\left\{\sum_{k=0}^{N-1} r_k(t - kT_{SYM})\exp(j2\pi f_k t)\right\} \tag{3.1}$$

where $\mathrm{Re}\{\cdot\}$ represents the real part of a complex variable, $r_k(t)$ is the complex baseband signal of the k^{th} OFDM symbol and is nonzero over the interval from 0 to T_{SYM}, N is the number of OFDM symbols, T_{SYM} is the symbol interval, and f_k is the center frequency for the k^{th} channel. The exact structure of the k^{th} OFDM symbol depends on its location within the packet:

$$r_k(t) = \begin{cases} r_{preamble,k}(t) & 0 \le k < N_{preamble} \\ r_{header,k-N_{preamble}}(t) & N_{preamble} \le k < N_{header} \\ r_{data,k-N_{preamble}}(t) & N_{header} \le k < N_{data} \end{cases}. \tag{3.2}$$

The structure of each component of $r_k(t)$ as well as the offsets $N_{preamble}$, N_{header}, and N_{data} will be described in more detail in the following sections.

All of the OFDM symbols $r_k(t)$ can be constructed using an inverse Fourier transform with a certain set of coefficient C_n, where the coefficients are defined as either data, pilots, or training symbols:

$$r_k(t) = \begin{cases} \sum_{n=-N_{ST}/2}^{N_{ST}/2} C_n \exp(j2\pi n\Delta_f (t - T_{CP})) & t \in [0, T_{FFT} + T_{CP}] \\ 0 & t \in [T_{FFT} + T_{CP}, T_{FFT} + T_{CP} + T_{GI}] \end{cases}. \tag{3.3}$$

The parameters Δ_f and N_{ST} are defined as the subcarrier frequency spacing and the number of total subcarriers used, respectively. The resulting waveform has a duration of $T_{FFT} = 1/\Delta_f$. Shifting the time by T_{CP} creates the "circular prefix" which is used in OFDM to mitigate the effects of multipath. The parameter T_{GI} is the guard interval duration.

3.3 Pilot Subcarriers

Two types of pilot signals are used in UWB system: standard pilots signals and user defined pilots signals. Standard pilot signals comply with the specification set forth, while the user defined pilot signals is left to the system designer.

In each OFDM symbol, there are twelve subcarriers are dedicated to the standard pilot signals. They are used to make coherent detection robust against frequency offsets and phase noise. These standard pilot signals are put in subcarriers –55, –45, –35, –25, –15 –5, 5, 15, 25, 35, 45, and 55. The standard pilot signals are BPSK modulated by a pseudo binary sequence to prevent the generation of spectral lines.

In OFDM symbol, the user-defined pilot signals are put in subcarriers –61, –60, …, –57, and 57, 58, …, 61. The user-defined pilot signals shall be BPSK modulated by the same pseudo binary sequence used to modulate the standard pilot signals.

3.4 OFDM Modulation

OFDM is seen as the modulation technique for future broadband wireless communications because it provides increased robustness against frequency selective fading and narrow band interference. OFDM is formed using Inverse Fast Fourier Transform (IFFT). In the receiver, the subcarriers are demodulated by using Fast Fourier Transformation (FFT). The high data rate of is achieved by combining many lower spead subcarriers to create one high speed channel. Subcarrier othogonality can be view in time and frequency domains. In frequency domain, the amplitiude spectra of individual subcarriers overlap which is shown in Figure 3-6. In time domain, each subcarrier must have an integer number of cycles in each OFDM symbol interval. Shown in Figure 3-7, the number of cycles between adjacent subcarriers differs by exactly one. Because OFDM receiver calculate the spectrum values at the maximum points of individual subcarriers, it can recover each subcarrier with inter carrier interference (ICI) from other subcarriers.

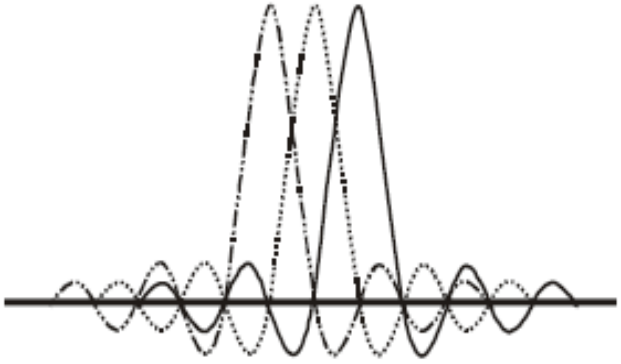

Figure 3-6 OFDM Spectra Containing 3 Subcarriers

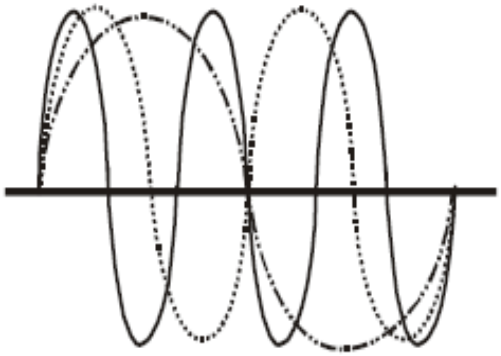

Figure 3-7 OFDM Symbol Containing 3 Subcarriers

For information data rates of 55 and 80 Mb/s, the stream of complex numbers is divided into groups of 25 complex numbers. For information data rates of 110, 160, and 200 Mb/s, the stream of complex numbers is divided into groups of 50 complex numbers. Complex numbers $c_{n,k}$ corresponds to subcarrier n of OFDM symbol k, defined in equation 3.5. For information data rates of 320 and 480 Mb/s, the stream of complex numbers is divided into groups of 100 complex numbers. Complex numbers $c_{n,k}$ corresponds to subcarrier n of OFDM symbol k. $c_{n,k}$ for data rate 55 and 80 Mb/s, data rate 110, 160, and 200 Mb/s and rates of 320 and 480 Mb/s are defined equation 3.4, equation 3.5 and equation 3.6 respectively [28].

$$\begin{aligned} c_{n,k} &= c_{(n+25),k} = d_{n+25\times k} \qquad n = 0,1,\ldots,24, k = 0,1,\ldots,\mathrm{N_{SYM}} - 1 \\ c_{(n+50),k} &= c_{(n+75),k} = d^{*}_{(24-n)+25\times k} \end{aligned} \tag{3.4}$$

where N_{SYM} is the number of OFDM symbols in the MAC frame body, tail bits, and pad bit.

$$\begin{aligned} c_{n,k} &= d_{n+50\times k} \qquad n = 0,1,\ldots,49, k = 0,1,\ldots,\mathrm{N_{SYM}} - 1 \\ c_{(n+50),k} &= d^{*}_{(49-n)+50\times k} \end{aligned} \tag{3.5}$$

where N_{SYM} denotes the number of OFDM symbols in the MAC frame body, tail bits, and pad bits.

$$c_{n,k} = d_{n+100\times k} \qquad n = 0,1,\ldots,99, k = 0,1,\ldots,\mathrm{N_{SYM}} - 1 \tag{3.6}$$

where N_{SYM} denotes the number of OFDM symbols in the MAC frame body, tail bits, and pad bits.

An OFDM symbol $r_{data,k}(t)$ is defined as equation 3.7.

$$r_{data,k}(t) = \sum_{n=0}^{N_{SD}} c_{n,k} \exp(j2\pi M(k)\Delta_F(t - T_{CP})) + p_k \sum_{n=-N_{ST}/2}^{N_{ST}/2} P_n \exp(j2\pi k\Delta_F(t - T_{CP})) \tag{3.7}$$

where N_{SD} is the number of data subcarriers, and N_{ST} is the number of total subcarriers used, and where the function *M(k)* defines a mapping from the indices 0 to 99 to the logical frequency offset indices –56 to 56, excluding the locations reserved for the pilot subcarriers and the DC subcarrier. The contribution due to the standard pilot subcarriers for the k^{th} OFDM symbol is given by the inverse Fourier Transform of the sequence P as in equation 3.8.

$$\mathrm{P}(k) = \begin{cases} \dfrac{1+j}{\sqrt{2}} & k = \pm 5, \pm 25 \\ \dfrac{-1-j}{\sqrt{2}} & k = \pm 15, \pm 35, \pm 45, \pm 55 \\ 0 & k = \pm 1, \ldots, \pm 4, \pm 6, \ldots, \pm 14, \pm 16, \ldots, \pm 24, \pm 36, \ldots, \pm 44, \pm 46, \ldots, \pm 54, \pm 56 \end{cases} \tag{3.8}$$

The subcarrier frequency allocation is shown in Figure 3-8. To avoid difficulties in DAC and ADC offsets and carrier feed-through in the RF system, the subcarrier falling at DC (0^{th} subcarrier) is not used.

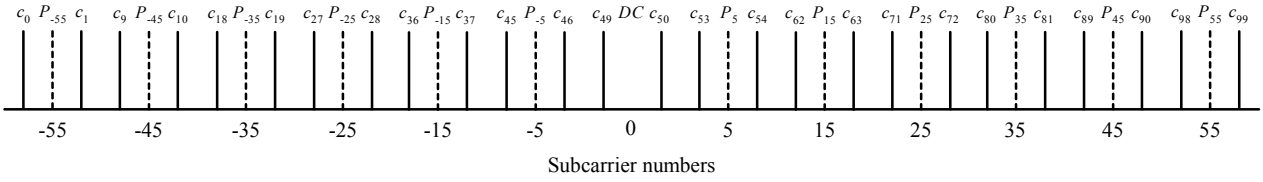

Figure 3-8 – Subcarrier Frequency Allocation [28]

3.5 Service Parameter Specific to UWB

In this section we list service parameters specific to UWB system. Table 3-1 lists data rate dependent modulation parameters for UWB system [28].

Table 3-1 Rate Dependent Parameters

Data Rate (Mb/s)	Modulation	Coding rate (R)	Conjugate Symmetric Input to IFFT	Spreading Across Tones	Spreading Gain	Coded bits per OFDM symbol (N_{CBPS})	Data bits per OFDM symbol (N_{DBPS})
55	QPSK	11/32	Yes	Yes	4	50	17.1875
80	QPSK	½	Yes	Yes	4	50	25
110	QPSK	11/32	Yes	No	2	100	34.375
160	QPSK	½	Yes	No	2	100	50
200	QPSK	5/8	Yes	No	2	100	62.5
320	QPSK	½	No	No	1	200	100
480	QPSK	¾	No	No	1	200	150

Table 3-2 lists of the timing parameters associated with the OFDM PHY.

Table 3-2 Timing Related Parameters

Parameter	Value
N_{SD}: Number of data subcarriers	100
N_{SDP}: Number of defined pilot carriers	12
N_{SUP}: Number of undefined pilot carriers	10
N_{ST}: Number of total subcarriers used	122 (= N_{SD} + N_{SDP} + N_{SUP})
Δ_F: Subcarrier frequency spacing	4.125 MHz (= 528 MHz/128)
T_{FFT}: IFFT/FFT period	242.42 ns ($1/\Delta_F$)
T_{CP}: Cyclic prefix duration	60.61 ns (= 32/528 MHz)
T_{GI}: Guard interval duration	9.47 ns (= 5/528 MHz)
T_{SYM}: Symbol interval	312.5 ns (T_{CP} + T_{FFT} + T_{GI})
$T_{PREAMBLE}$: PLCP preamble duration	9.375 μs

3.6 UWB ROF Technologies

The UWB RoF system generally consists of commonly used components such as light sources, photo-detectors, modulators, optical fibers, etc. The components that make up UWB RoF system can be classified as active and passive components.

The UWB RoF modulation that convert wireless signal to optical domain can be direct modulation of different types of lasers or external modulation. Several aspects must be taken into account with the purpose to choose an appropriate solution such as: broadening of the chirped signal due the dispersion in optical fiber. The external modulation has the advantage of no laser chirping due to the modulation. How ever RoF system using direct modulation has much simplified design and lower cost. Over the years, the requirements for long-haul system capacity have been steadily increased, as has the need to improve laser diode quality. In response, quantum well and distributed feedback laser diodes (DFB) with extremely narrow spectral width of an order of tenths of nanometers have been developed. Vertical cavity surface emitting lasers (VCSEL) and quantum dot based lasers are among the recent developments of light sources. Recently, [23] explored the performance of ROF for the distribution of WLAN (802.11a and

802.11g) concurrently with Gigabit Ethernet (GbE) and OFDM signals using low-cost 850nm VCSEL in multimode fiber. It is concluded that RoF can support these services using low-cost VCSEL. The great challenge of technical research and development is to realize low-cost devices and design high quality networks on a low cost level.

Chapter 4 Optical Communication System

The optical communication system in this research is composed of laser light source, modulator, optical fiber, and PIN diode. There are two main technologies to optically distributing RF signals: externally modulated and direct modulated. For external modulation of laser shown in Figure 4-2, electro-optic modulator such as Mach-Zehnde Modulator (MZM) is used to intensity modulate the laser output with the modulating signal. For direct modulation of laser shown in Figure 4-1, the laser diode's current is directly modulated. With external modulation the laser bias current is held constant and the Relative Intensity Noise (RIN) is low of laser and can achieve greater performance in RoF application compares with direct modulation. However direct modulation method is simple in design and is low cost. In this study, direct modulated Vertical Cavity Surface Emitting Laser (VCSEL) is used for cost effective UWB RoF system.

Figure 4-1 Direct Modulation of Laser [29]

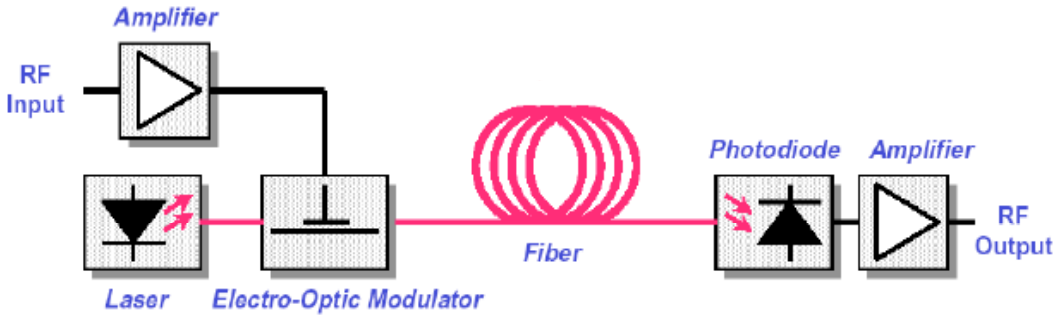

Figure 4-2 External Modulation of Laser [29]

4.1 VCSEL Dynamics

The VCSEL has advantages for low-cost data transmission. The use of a laser means that multi-gigahertz modulation is possible, and the stimulated emission is directional, rather than the isotropic spontaneous emission of LEDs. Because the light is emitted directly from the surface, single or multimode fiber can be directly buttcoupled with an inexpensive mounting technology, and the coupling efficiency can be very high. The VCSELs can also be fabricated in linear arrays that can be coupled inexpensively to linear arrays of fibers for parallel fiber interconnects with aggregate bit rates of several gigabits per second, amortizing the alignment cost over the number of elements in the array. VCSELs lend themselves to two-dimensional arrays as well, which makes them attractive to use with smart pixels. The planar fabrication of VCSELs allows for wafer-scale testing, another cost savings.

Standard oxide confined 850 nm VCSELs under direct high-frequency modulation is used in this study for fiber optic RF links in wireless communication. Such VCSELs represent a mature technology and are readily available.

4.1.1 Power/Voltage vs. Current Characteristics

The VCSEL have similar P-I performance to edge-emitting laser diodes, with some small differences (See Figure 4-3). Because the acceptance angle for the mode is higher than in edge emitting diodes, there will be more spontaneous emission. The operating voltage is 2 to 3 times that of edge-emitting lasers. The common expression for the P-I curve above threshold is given by 4.1 [42].

$$P_o = \eta_S (I - I_{th}) = \eta_d \frac{hv}{q}(I - I_{th}) = \eta_i \frac{\alpha_m}{\alpha_i + \alpha_m}\frac{hv}{q}(I - I_{th}) \tag{4.1}$$

Where I_{th} is the threshold current, I is the operation current, η_s is slope efficiency, η_d is differential quantum efficiency, q is electron charge, hv is photon energy, α_i is photon losses, α_m is the mirror loss parameter.

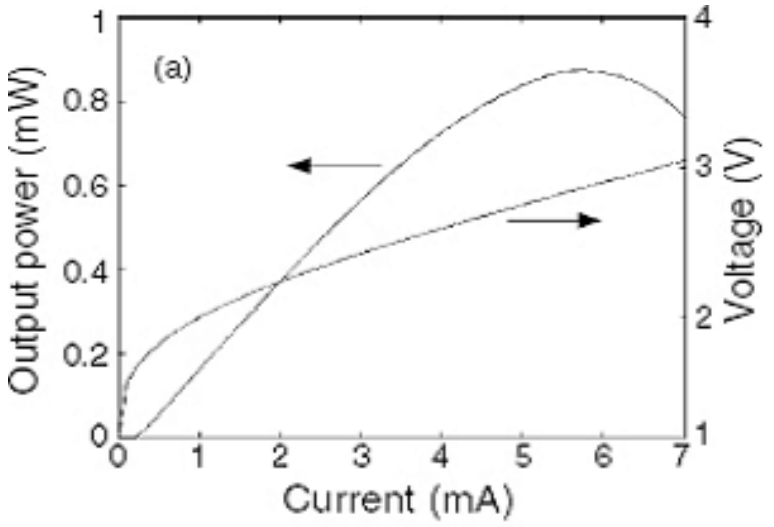

Figure 4-3 Power vs. Current for VCSEL [29]

4.1.2 Modulation Response

The frequency-dependent modulation response of a semiconductor laser can be described by the following three-pole transfer function [29]. The modulation can be illustrated in equation 4.2, in which the first part, containing two complex-conjugate poles, represents the intrinsic carrier–photon interaction (second-order system) with resonance frequency f_r and damping rate γ. The second part containing a real pole represents additional extrinsic limitations due to carrier transport and parasitic elements related to the laser structure, where f_p is the cut-off frequency of the low-pass filter characterizing the extrinsic limitation.

$$H(f) = const\left(\frac{f^2}{f_r^2 - f^2 + j\left(\gamma/2\pi\right)f}\right)\left(\frac{1}{1 + j\,f/f_p}\right) \tag{4.2}$$

Simulated modulation response at different bias current for VCSEL is shown in Figure 4-4. This figure also shows relaxation oscillation peak. The indices from (a) to (g) correspond to bias current of 0.4, 0.55, 0.8, 1.25, 2.5, 3.6, and 5 mA respectively.

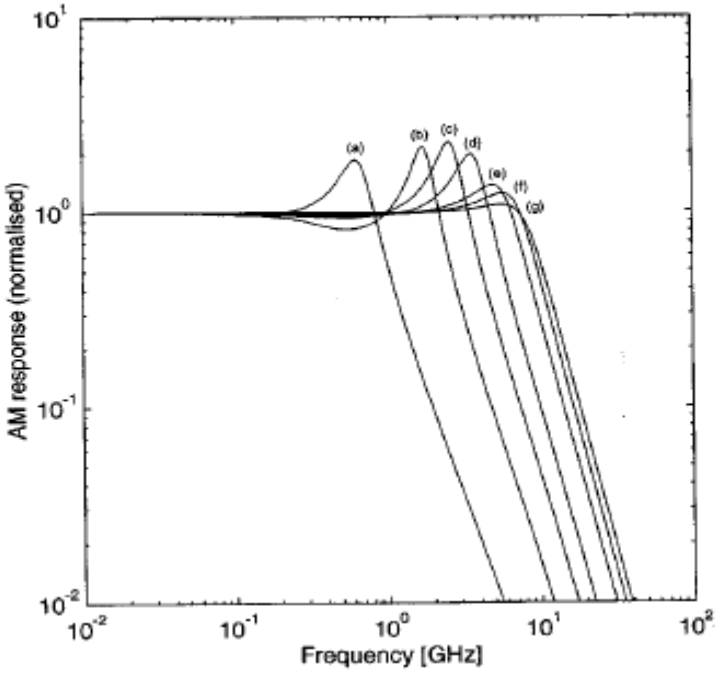

Figure 4-4 Modulation Response at Different Bias Currents [29]

We can conduct a rate equation analysis. It is shown in equation 4.3, that the damping rate is proportional to the square of the resonance frequency [29].

$$\gamma = Kf_r^2 + \frac{1}{X\tau_n} \tag{4.3}$$

where τ_n is the differential carrier lifetime and X a factor that accounts for carrier transport effects.

The damping rate can be plotted as a function of the square of the resonance frequency. equation 4.4 shows that the *K*-factor can be determined for a given VCSEL. The *K*-factor can then be used to estimate the maximum intrinsic bandwidth (damping limited) in the absence of other limitations [29].

$$f_{3dB,damping} = \frac{2\pi\sqrt{2}}{K} \tag{4.4}$$

When the bias currents are high, the resonance frequency may saturate and reach a maximum value of $f_{r,\max}$ due to thermal effects. In the absence of other limitations, the maximum modulation bandwidth (thermally limited) is given by equation 4.5 [29].

$$f_{3dB,thermal} = \sqrt{1+\sqrt{2}f_{r,\max}} \tag{4.5}$$

In the absence of damping and thermal limitations, the maximum modulation bandwidth, limited by parasitic and transport effects, is given by equation 4.6 [29].

$$f_{3dB,parasitic} = (2+\sqrt{3})f_p \tag{4.6}$$

The modulation bandwidth is limited by combination of damping, thermal and parasitic effect. From a rate equation analysis D-factor can be expressed as equation 4.7. A laser used in an analogue link should be modulated at a frequency considerably below the resonance frequency since both noise and distortion attain their maximum values at the resonance frequency. A parameter of great importance is the rate at which the resonance frequency increases with current above threshold [30].

$$f_r = D\sqrt{I - I_{th}} \tag{4.7}$$

where I is the bias current and I_{th} is the threshold current.

4.1.3 Relative Intensity Noise

The quantum nature of electrons and photons and the random nature of physical processes produce random fluctuations (noise) of the output power, even without current modulation. For

analog applications, intensity noise is quantified using the signal-to-noise ratio (SNR) which is linked to the Relative Intensity Noise (RIN) commonly used with laser diodes: $SNR = m^2 / 2RIN$ [22]. In single mode operation, RIN is almost constant at lower RF frequencies and it peaks at the laser resonance frequency. Higher output power gives lower RIN (Figure 4-5).

$$\frac{RIN_{RF}}{\Delta f} = \frac{(\delta P)^2}{\Delta f P_0^2} = \frac{4h\nu V_a \alpha_m v_g \beta R_{sp}}{\omega_r^4 \tau_t^2 P_o} + \frac{2h\nu}{P_o}\left[\eta_0 \frac{I + I_{th}}{I - I_{th}} + 1 - \eta_o\right] \tag{4.8}$$

Where V_a is averaged over the active volume, α_m is photon emission mirror loss, v_g photon group velocity, β is the fraction of spontaneously emitted photons that enter the lasing mode, R_{sp} is the spontaneous emission rate, $h\nu$ is photon energy, P_o is output power, ω_r is angular electron–photon resonance frequency, τ_t is the transport time constant, I_{th} is the threshold current.

The first term in equation 4.8 is due to spontaneous emission and it decreases as $1/P^3\omega_r^4\partial P_0^4$. The second term dominates with high output power P_o and it is caused by the shot noise of the injected current.

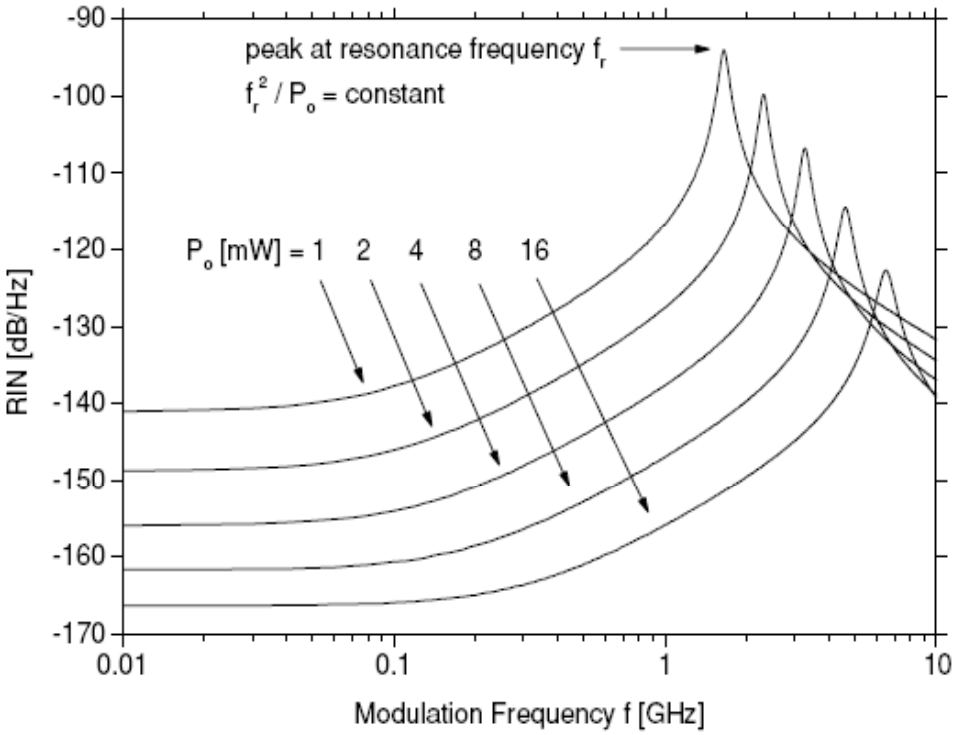

Figure 4-5 RIN at Different DC Output Power Levels [22]

Lower output power and unstable polarization of VCSELs causes higher noise than with in-plane lasers, especially with polarization sensitive applications. However, polarization controlled VCSELs have shown RIN below −140 dB/Hz. VCSEL noise was found to be less sensitive to external feedback than with in-plane lasers [38].

The intrinsic intensity noise of a semiconductor laser is quantified using the relative intensity noise (*RIN*) defined as equation 4.9 [29].

$$RIN = \frac{(\delta P(t)^2)}{P_0^2} \tag{4.9}$$

where P_0 is the average power and $\delta P(t)^2$ denotes the mean square power fluctuation.

From a small-signal analysis of the rate equations for a single-mode laser, with the driving force being the spontaneous emission, the RIN spectrum attains the following frequency dependence given by equation 4.10 [29].

$$RIN(f) = \frac{Af^r + B}{(f_r^2 - f^2)^2 + (\gamma / 2\pi)^2 f^2} \tag{4.10}$$

which shows that *RIN* peaks at the resonance frequency.

Intensity noise spectra contain both the laser RIN and the shot noise, with the equivalent shot noise RIN given by equation 4.11.

$$RIN_s(f) = \frac{2q}{I_0} = \frac{2q}{RP_0} \tag{4.11}$$

where I_0 is the dc-photocurrent in the optical receiver and R is the detector responsivity.

4.1.4 Inter-modulation Distortion

Harmonic distortion describes the output at harmonics of the modulation frequency (with the n^{th}-order harmonic distortion describing the output at the n-th harmonic). Inter-modulation distortion describes the output at the sum and difference frequencies when the current modulation contains several frequencies. See Figure 4-6 for calculated ac output spectrum with f=1 GHz modulation frequency [42].

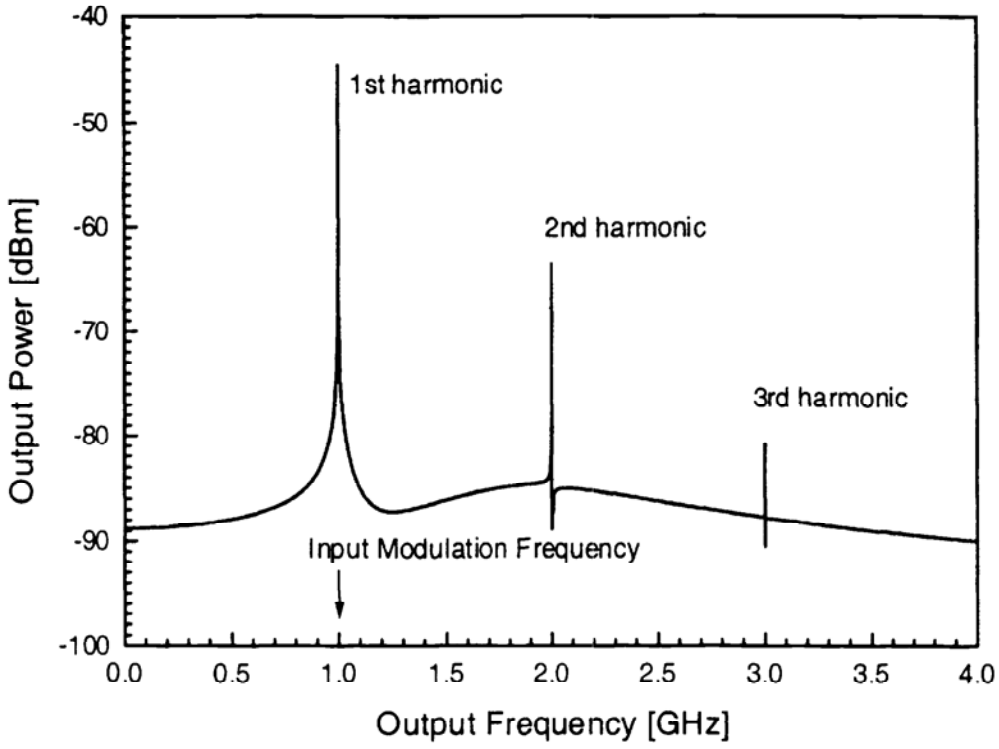

Figure 4-6 Calculated AC Output Spectrum Modulation Frequency at 1 GHz [29]

A sinusoidal current modulation generates light power modulations at the input frequency ω and also at the harmonics 2 ω, 3 ω,....$n\,\omega$. The amplitude of the *n*th order harmonic is proportional to the *n*th power of the optical modulation depth $|\Delta P(\omega)|/P_o = m|M(\omega)|$ and it decreases rapidly with higher order. Harmonic distortion (HD) depends on the nonlinearity of a transmission system. In the case of laser diodes, it is often related to the nonlinearity of the P-I characteristic, which can be expressed by the Taylor series given by equation 4.12.

$$P(I) = P(I_0) + (I - I_0)\frac{\partial P}{\partial I} + \frac{1}{2}(I - I_0)^2 \frac{\partial^2 P}{\partial I^2} + \frac{1}{6}(I - I_0)^3 \frac{\partial 3P}{\partial I^3} + \ldots \qquad (4.12)$$

With analog modulation, the last two terms of equation 4.12 yield second and third order distortions. Even with perfectly linear PI characteristics, distortions are generated by the intrinsic interaction of electrons and photons during stimulated recombination. This can easily be

recognized from the $N \times S$ terms in the linearized rate equations which generate time dependences exp($i2\,\omega t$), exp($i3\,\omega t$), etc., in addition to the exp($i\,\omega t$) dependence described earlier. Intrinsic distortion dominates at frequencies near the resonance frequency f_r and often limits the usable bandwidth to low frequencies $f \langle\langle f_r$. Intermodulation distortion arises when two or more signals at different modulation frequencies are transmitted. Two signals at ω_1 and ω_2, for example, are accompanied by second order distortions at frequencies $2\,\omega_{1,2}$ and $\omega_1 \pm \omega_2$, third order distortions at frequencies $3\,\omega_{1,2}$, $2\,\omega_1 \pm \omega_2$, and $2\,\omega_2 \pm \omega_1$, etc. The third order inter-modulation distortions (IMDs) at $2\,\omega_1 - \omega_2$ and $2\,\omega_2 - \omega_1$ are of special interest since they are close to the original signals and they might interfere with other signals in multi-channel applications (Figure 4-7). The set illustrates the variety of distortions of the AC output spectrum. The dotted lines give the decay of intrinsic distortions with lower frequencies. The third order IMD increases as the cube of the modulation depth. The amplitudes of inter-modulation distortions can be related to the amplitudes of harmonic distortions (those relations depend on the dominating cause of the distortion: intrinsic or static distortion). In multi-channel applications, distortions from several channels add up and they are described by composite second order (CSO) and composite triple beat (CTB) quantities. Additional distortions from clipping occur when the combined modulation depth of all channels is larger than one, i.e., when the total modulation current drops below the threshold current [27].

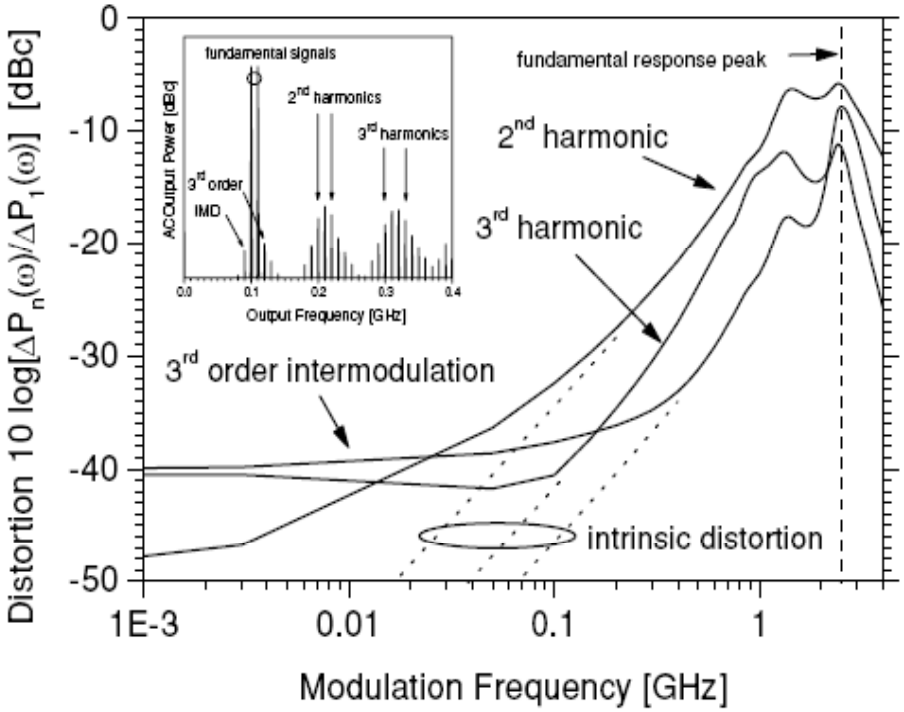

Figure 4-7 Harmonic and Inter-modulation Distortions vs. Modulation Frequency [27]

Besides internal mechanisms, external feedback can affect the strength of laser distortion substantially. This type of distortion is proportional to the amount of feedback entering the laser and it exhibits periodic changes with increasing modulation frequency ω (amplitude $\propto \omega^{-1}$) [34]. Optical isolators are commonly used to reduce feedback effects.

4.1.5 Dynamic Range

The dynamic range of linearity is of great importance for many analog modulation applications. Even if the total lasing power changes linearly with injection current, intrinsic distortions draw power from the fundamental signal. At low modulation depth, distortions are still below the noise floor but the signal-to-noise ratio is also small. With increasing modulation depth, distortions rise above the noise floor and grow faster than the fundamental signal. Thus, the largest distortion free signal-to-noise ratio (dynamic range) is reached when the amplitude of the distortion is equal to the noise floor. Figure 4-8 shows the effect of changing the modulation

depth M at I=4mA. 1st, 2nd and 3rd order harmonics, respectively, are expected to be the first components of a power series $P_{out} = a_1 P_{in} + a_2 P_{in}^2 + a_3 P_{in}^3 ...$ with P_{in} being the input ac signal power and P_{out} being the total ac output power [42]. Since the noise floor depends on the measurement bandwidth Δf, the spurious free dynamic range SFDR refers to Δf = 1 Hz. SFDR is the same for input and output. External optical feedback can cause the SFDR to vary periodically with changing modulation frequency [39]. Pre-distortion of the input signal used to increase the inter-modulation-free dynamic range of VCSEL laser diodes is discussed in 6.1.2.4.

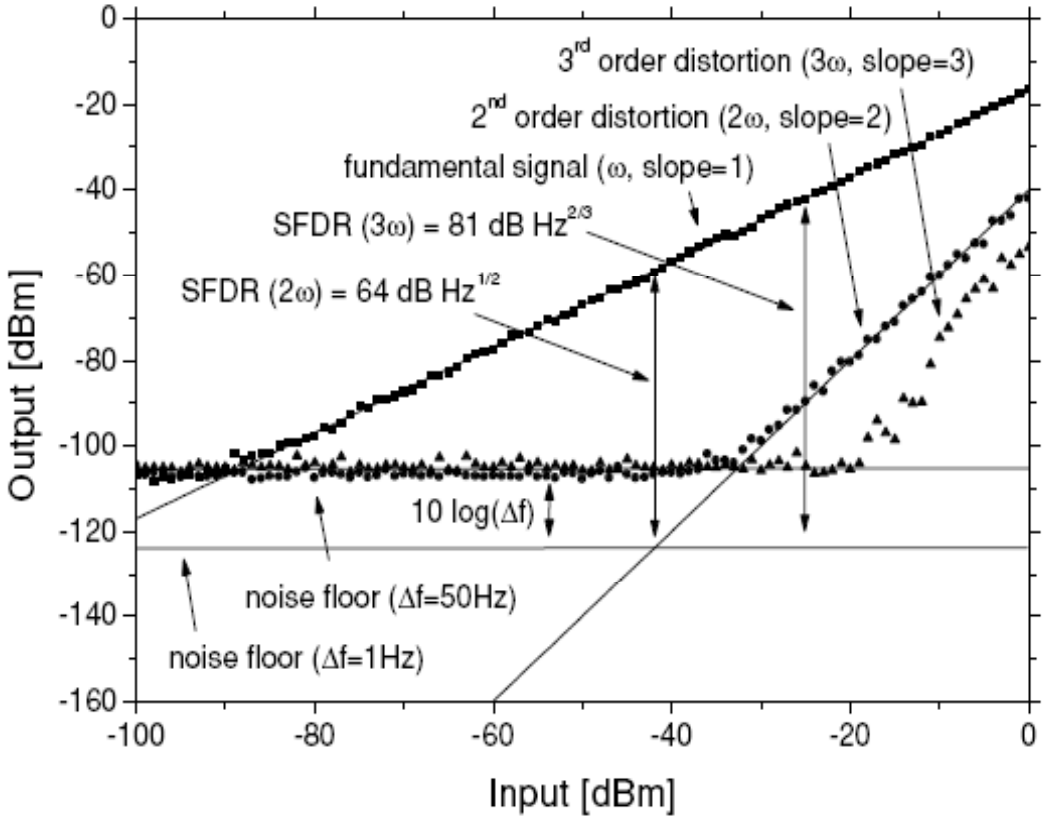

Figure 4-8 1.55 μm VCESL Output Power (dots) versus Input Power [42]

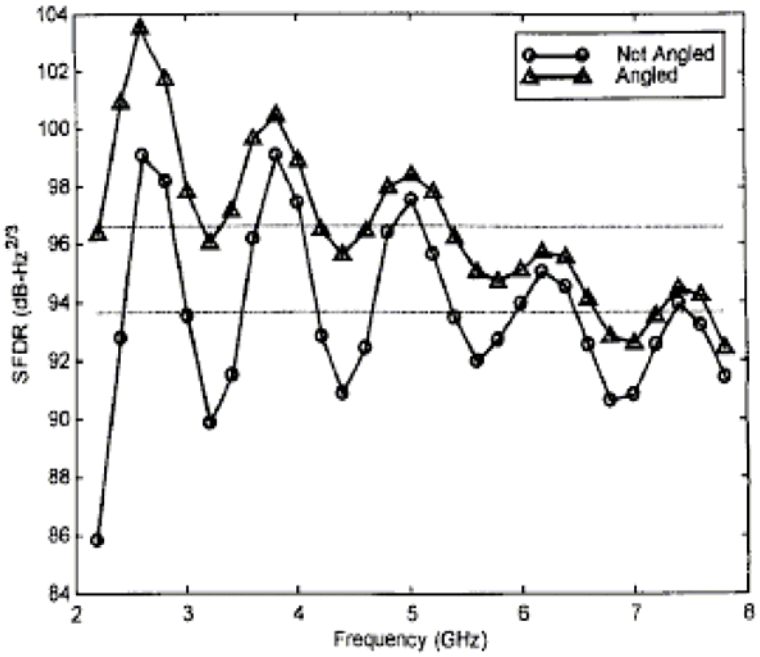

Figure 4-9 SFDR for the 10 mm Device at l0 mA Bias [42]

Figure 4-8 gives the first results on the SFDR for HD-free operation of 1.55 μm VCSELs at 1 GHz modulation frequency [42]. Lines illustrate the extraction of the spurious free dynamic range (SFDR) for second and third order harmonic distortion. Figure 4-9 reviews the maximum inter-modulation-free SFDR as measured at different modulation frequencies. Dashed lines are average values of SFDR across the frequency range. For the angled case, the oscillations are reduced and the average SFDR improves by approximately 3dB IMD3. The decline with higher frequency reflects the enhancement of intrinsic distortion close to the resonance frequency. However, there is no further increase of SFDR with lower frequencies. To achieve a large dynamic range, it is advantageous to use laser designs with high differential gain (strained quantum wells) and low photon lifetime (low mirror reflectivity).

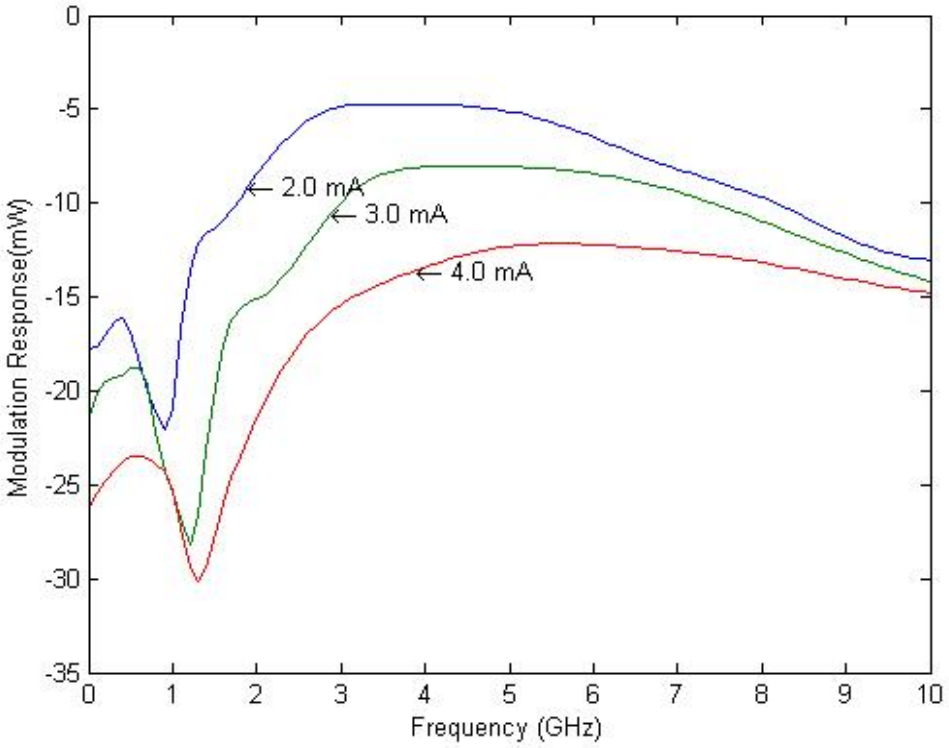

Figure 4-10 Single Mode VCSEL Second Order Harmonic Distortion

Non-linearity in the response of the VCSEL causes distortion of the analogue signal. Major sources of distortion are the intrinsic non-linearity associated with the relaxation oscillations and spatial hole-burning-induced distortion [45]. To illustrate these phenomena, and their frequency dependences, we show in Figure 4-10 calculated second-order harmonic distortion for a single VCSEL at different bias currents. At modulation frequencies near the resonance frequency, the distortion peaks due to the intrinsic non-linearity associated with the relaxation oscillations.

4.1.6 Impedance Matching

Most of the VCSEL driver is designed for particular impedance, whether directly attached or at the end of a transmission line. In either case, if the VCSEL, line, and driver are not matched, the interactions lead to anomalous waveforms. Just how well matched the system must be depends on many factors, but it is wise to aim for no worse than a 10% mismatch.

4.2 Optical Fiber

In this section we discuss properties of optical fiber.

4.2.1 Fiber Attenuation

Fiber attenuation in fiber results from a variety of causes. Fiber attenuation occurs due to fundamental scattering processes (the most important contribution is Rayleigh scattering), absorption (both the OH-absorption and the long-wavelength vibrational absorption), and scattering due to in-homogeneities arising in the fabrication process. Attenuation limits both the short and long-wavelength applications of optical fibers. Figure 6 illustrates the attenuation characteristics of a typical fiber. Attenuation limits both the short and long-wavelength applications of optical fibers. Figure 4-11 illustrates the attenuation characteristics of a typical fiber. Fiber attenuation in fiber depends on the wavelength of operation [13]. For optical fiber communications, two windows or range of wavelengths are used. One is 1310 nm window and the other is1500 nm window. At 1310 nm fiber dispersion is zero. However, at 1550 nm fiber loss is minimum. These two are contradicting requirements. There are fibers, which are manufactured in such a way that they possess minimum dispersion at 1550 nm.

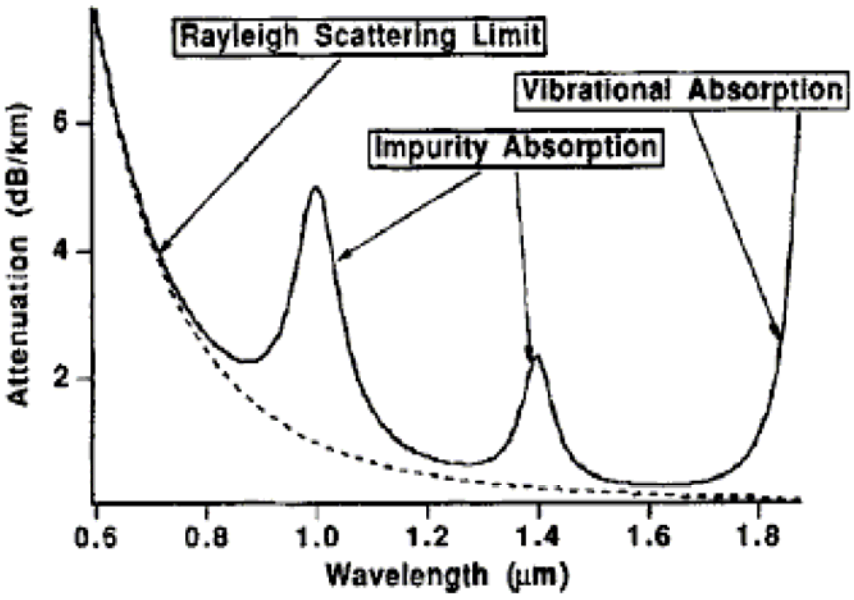

Figure 4-11 Fiber Attenuation [13]

4.2.2 Fiber Dispersion

Four major dispersion mechanisms are present in fiber optic transmission.

4.2.2.1 Chromatic Dispersion

Chromatic dispersion refers to the wavelength-dependent pulse spreading that occurs as the optical signal propagates along the fiber. There are two contributing factors to chromatic dispersion. The first one is the dependence of the fiber material's refractive index on the wavelength – referred to as material dispersion. The second factor is the waveguide dispersion, which occurs as a result of the dependency of the propagation constant on the wavelength. The end result is that different spectral components arrive at slightly different times, leading to wavelength-dependent pulse spreading, or dispersion. In many instances, material dispersion is the main contributor to chromatic dispersion. The pulse spreading due to chromatic dispersion is then given by

$$\Delta\lambda_{chrom} = D(\lambda) * \Delta\lambda * L \tag{4.13}$$

where $D(\lambda)$ is the dispersion parameter (in ps/nm * km), $\Delta\lambda$ is the spectral width of the light source, and L is the length of the fiber. Thus, the broader the spectral width is, the greater the dispersion. For silica fibers, the dispersion parameter, $D(\lambda)$ may be approximated by the Sellmeier [41].

$$D(\lambda) = \frac{S_0}{4}\left[\lambda - \frac{\lambda_0^4}{\lambda^3}\right] \tag{4.14}$$

where S_0 is the zero dispersion slope, and λ_0 is the zero-dispersion wavelength, which occurs around 1300 nm. Typical dispersion parameter, $D(\lambda)$ values of silica fibers are -3 ps/nm*km, and -17 ps/nm*km at 1310 nm and 1550 nm respectively [41].

Chromatic dispersion is negligible across the band in case of analog optical link due to the narrow bandwidth occupancy of the analog signal compared to the optical carrier frequency.

However, this is not true across the two sidebands. The variation in-group delay between the two sidebands of an analog double-sideband modulated signal can be significant, particularly if the RF carrier frequency is large. The difference in-group delay between the two sidebands causes their phases to rotate with respect to one another. The resulting constructive and destructive interference between the two sidebands causes the power in the detected signal to vary in a fading pattern, which is a function of the fiber length traversed [43]. The fading profiles due to chromatic dispersion with λ=1550 nm and D = 17 ps/(nm/km) are plotted in Figure 4-12 for RF carrier frequencies of 15 GHz. The first null in the fading profile at this frequency occurs when the signal has traveled over more than 100 km of fiber. There is less than 3 dB of attenuation when the distance traveled is not more than 50 km.

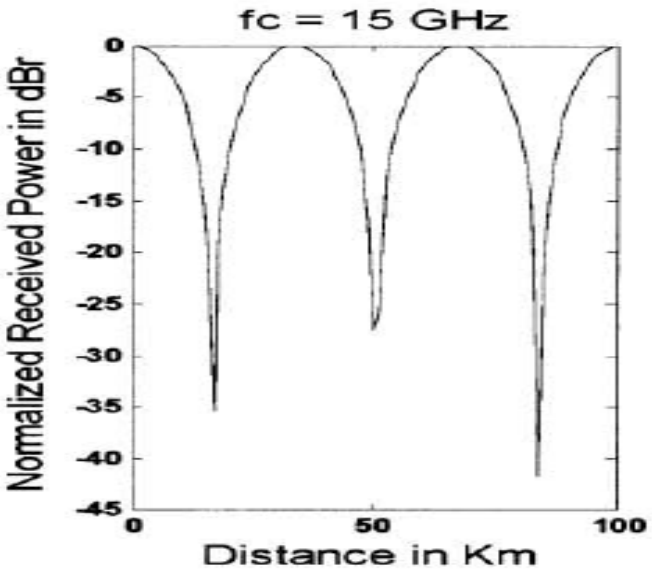

Figure 4-12 Chromic dispersion fading in fiber [43]

4.2.2.2 Modal Dispersion

The advantage of multimode fibers (MMFs) over single-mode fibers (SMFs), in general, is their relaxed coupling tolerance, thanks to their larger core diameters, which lead to reduced system-wide installation and maintenance costs. Traditionally, MMFs were made from silica. MMFs allow the propagation of multiple guided modes albeit with different propagation constants. The difference in the mode propagation times leads to intermodal dispersion, which severely limits

the fiber bandwidth. As a result of the limited bandwidth, coupled with the associated lower installation and maintenance costs, MMFs have been confined to short link applications such as LANs. Therefore, modal dispersion is the dominant performance-limiting factor in MMFs. The objective of the GI profile is to equalise the propagation times of the various propagating modes. The graded refractive index profile can be approximated by the power law equation given by equation 4.15.

$$n(r) = \sqrt{n_{cc}^2 * \left[1 - 2\Delta(\frac{r}{a})^q\right]}; 0 \le r \le a$$
$$n(r) = n_{cl}; r > a \tag{4.15}$$

where q is the index exponent, r corresponds to the cylindrical radial coordinate, n_{cc} and n_{cl} are the refractive indexes of the core centre and cladding respectively, a is the core radius, and Δ is the relative indices difference given by equation 4.16.

The refractive index profile is determined by the index exponent, q. If $q = 1$, a linear profile is obtained. If $q = 2$, a parabolic index profile is obtained, and the condition $q = \infty$ corresponds to a step index profile.

$$\Delta = \frac{n_{cc}^2 - n_{cl}^2}{2n_{cc}^2} \tag{4.16}$$

4.2.2.3 Mode Polarization Dispersion

The next significant component of an optical system is the optical fiber. The fiber may be simply modeled as a fixed attenuation per distance. A common type of fiber in use today is the Corning SMF-28 fiber. This fiber is specified to have an optical power loss of 0.19 dB/km at a wavelength of 1550 nm. There are fiber optic connectors available with return losses greater than 60 dB, and insertion loss less than 0.25 dB. If even better performance is required, fiber optical

cables can be fusion spliced together to get connections with insertion losses of around 0.02 dB, and return losses much larger than 60 dB.

Chapter 5 Non-Linear Effect of Optical System on OFDM

Transmission of analog wide band OFDM signals such as UWB has been limited by the linearity constraints in the modulating/demodulating devices and by the distortion effects created by the optical link. AM\AM distortions are a major focus of research with OFDM systems. Because of the large number of carriers used in an OFDM system especially for UWB, the dynamic range for the output of the RF signal can be quite large. Thus, researcher have been facing with the problem of minimizing the amount of harmonic distortions caused by driving the modulator into saturation yet maintaining an efficient operating point .The non-linearity causes two effects on the detected samples:

- Constellation warping of amplitude and phase distortions as shown in Figure 5-1 [44].
- Nonlinear distortion, which causes a cluster of received values around each constellation point rather than a single point.

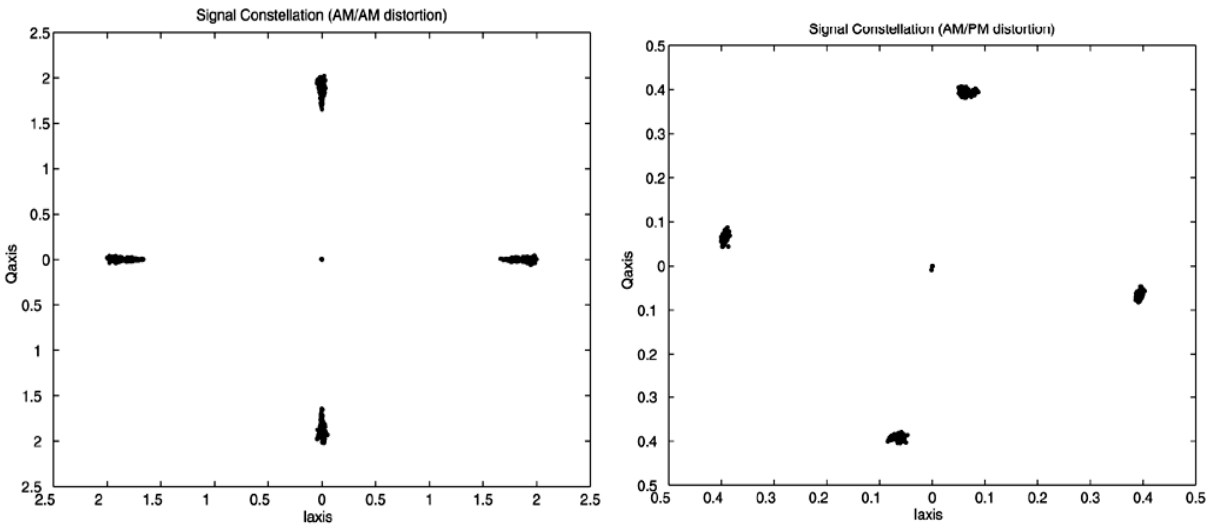

Figure 5-1 a) AM\AM distortion on a quaternary phase shifting keying signal. b) AM\PM distortions on a quaternary phase shifting keying signal [44]

The analysis in section Chapter 4 points out, RIN, second-order harmonic distortion, and third-order distortion affect the quality of UWB OFDM signal transmitted through the optical communication system. In this section design solution is proposed to mitigate no-linear effect caused by large peak-to-average power ratio (PAPR), which limits the peak amplitude of the

OFDM waveform and phase noise, which increases the SNR. Adaptive phase tracking and equalization applied to mitigate the non-linearity.

5.1 High Peak to Average Power Reduction

Because of the difficulty with filtering out near-in inter-modulation (IM) products, IM is the most difficult to deal with. Equally important situation is when the harmonic distortions are caused by the input signal driving the amplifier into its saturation region. In the saturation region, an increase in input drive level does not result in an increase in output power level. The definition for the beginning of the saturation region is specified relative to the 1 dB compression point. Shown in Figure 5-2, the 1 dB compression point is labeled "P1dB" and is defined as the point at which a 1 dB increase in input power results in 1 dB decrease in the linear gain of the analog device [44]. There for, the dynamic range of analog device, which also corresponds to the linear region of operation for an analog device, is defined between the noise-limited region and the saturation region.

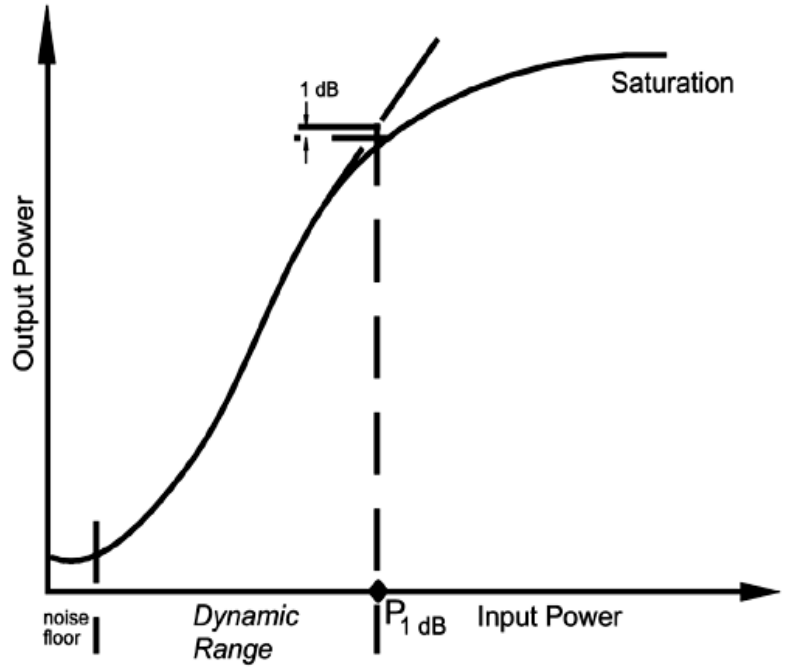

Figure 5-2 Power Transfer Function [44]

5.1.1 High Peak to Average Power of OFDM

Large peak-to-average ratio (PAPR) distorts the OFDM signal if the transmitter contains nonlinear components such as laser sources. The nonlinear effects on the transmitted OFDM symbols are spectral spreading, inter-modulation, and changing the signal constellation. In other words, the nonlinear distortion causes both in-band and out-of-band interference to signals. The in-band interference increases the BER of the received signal through warping of the signal constellation and inter-modulation while the out-of-band interference causes adjacent channel interference through spectral spreading. The latter is what prevents the usage of OFDM in many systems even if the in-band interference is tolerable [31]. Therefore the laser source requires a backoff, which is approximately equal to the PAPR for distortionless transmission. So, reducing the PAPR is of practical interest. The OFDM baseband signal for N subcarriers is:

$$x(t) = \sum_{n=1}^{N} a_n \cos \omega_n t + jb_n \sin \omega_n t \tag{5.1}$$

where the a_n and b_n are the in-phase and quadrature modulating symbols.

If each carrier has amplitude A, the maximum PAPR will be: (NA)^2 / [N*(A^2/2)] = 2N When the number of subcarriers N is small, a PAPR of 2N has reasonable chances of occurring. However, if N is large enough so that the central limit theorem applies, the amplitude distribution of the OFDM signal is better approximated by a Rayleigh distribution since a PAPR of 2N has exceedingly small probability of occurring. The cumulative distribution function for the peak power per OFDM symbol is shown in equation 5.2 [18].

$$P(z) = (1 - \exp(-\frac{1}{2}.\frac{z}{\delta^2}))^N \tag{5.2}$$

where z is the complex envelope power of x(t) and $\frac{z}{\delta^2}$ represents envelope power to average symbol power ratio.

The plot of CDF distribution [18] is shown in Figure 5-3.

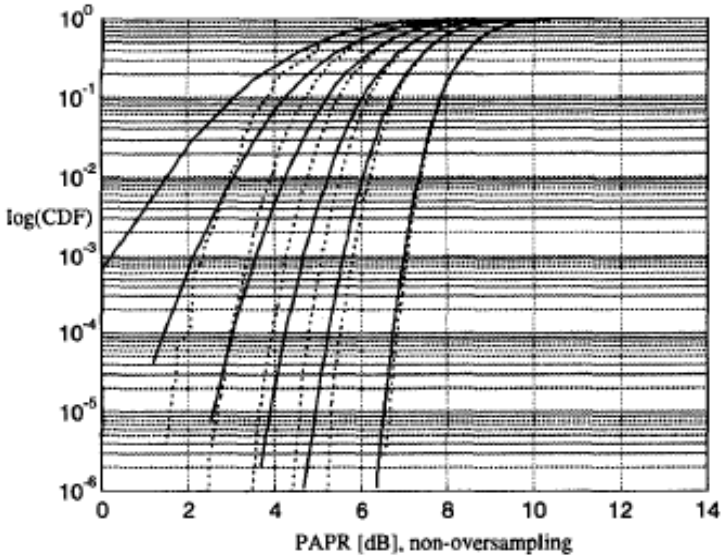

Figure 5-3 CDF for (left to right) N=16, 32, 64, 128, 256 and 1024 (solid Line is simulated)

As can be seen from the graph, high PAPR does not occur often. The in-band interference is caused by the nonlinearity results in a warping (a rotation and magnitude gain) of the received constellation in Figure 5-4.

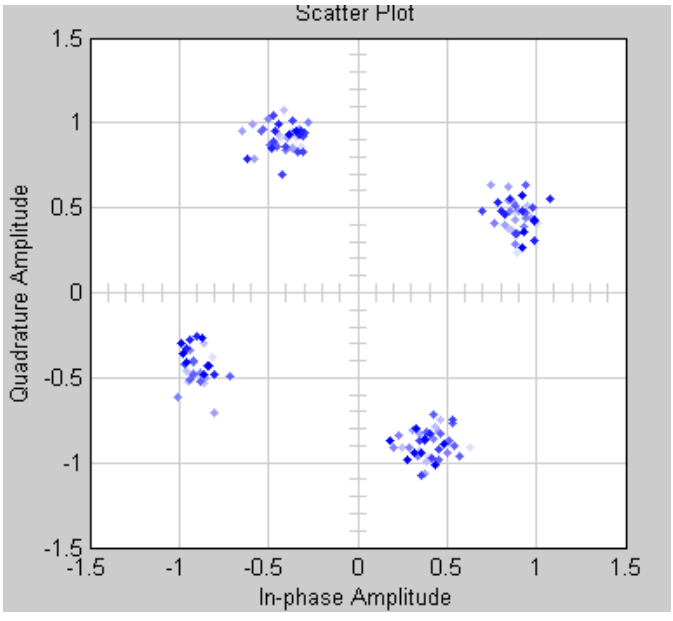

Figure 5-4 Signal Constellation at the Output of FFT for QPSK, N = 128

The spectral spreading effect is also plotted for N = 128 in Figure 5-5.

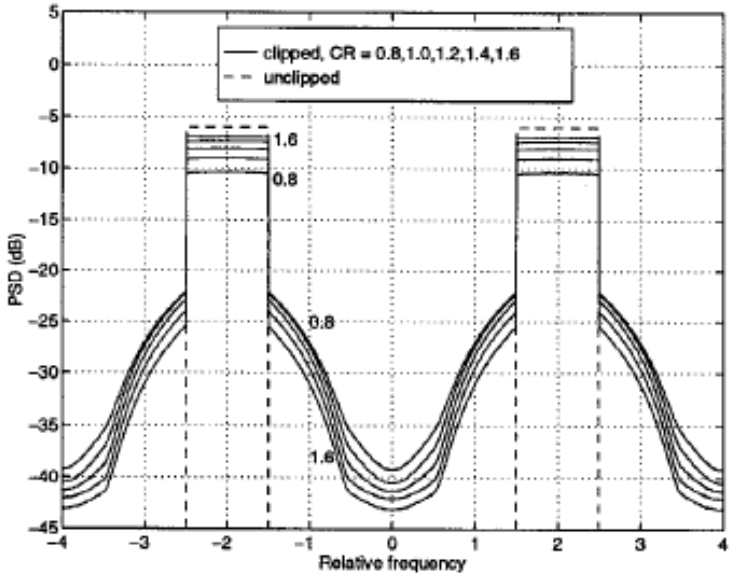

Figure 5-5 Power Spectral Density of the Clipped and Filtered OFDM Signals with CR=1.4

5.1.2 PAPR Reduction Methods

Pre-distortion techniques are used to compensate for non-linear distortions by modifying the input signal characteristics. The pre-distortion techniques can be either non-adaptive or adaptive. We will discuss these techniques in this section. But the most common non-adaptive technique studied in the literature and used in practice is amplitude clipping. Amplitude clipping limits the peak envelope of the input signal to a predetermined value, otherwise the input signal through without change.

5.1.2.1 Adding Artificial Signals

When transmitting M-point FFT and IFFT, not all M frequencies carry data, only N < M number of carriers actually contain data. So, there are a few empty carriers per OFDM symbol. This technique is adding sine waves at these empty carrier frequencies in a way so that the composite OFDM symbol will have a lower PAPR. A desired maximum value is set for the envelope to be C and equate this to the expression for the envelope of the composite signal for one or two artificial signals [36]. The amplitudes, phases and frequencies of these artificial signals are

found if the equation has valid roots. Adding two artificial signals, the PAPR can be reduced by 6 dB for 16 carriers. The result is in the graph Figure 5-6. But using this method requires computing a convex optimization problem for every OFDM symbol. With the increasing computational power and proper algorithms, these solutions may be implemented efficiently.

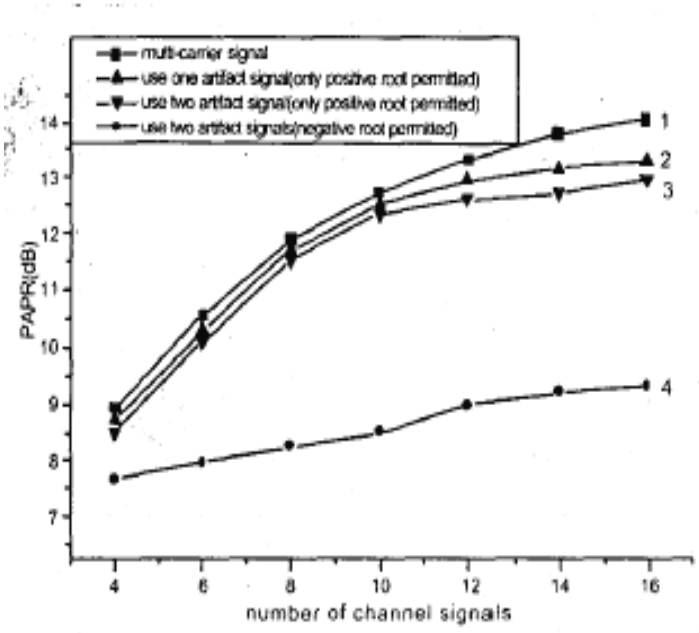

Figure 5-6 Comparison of PAPR Under Different Conditions [36]

5.1.2.2 Redundant Coding

In this method, redundant bits are appended with data bits to form a message symbol. So distortion is not introduced to the signals. The premise is, all possible message symbols, only those with low peak power will be chosen by coding as valid code words for transmission [24]. N subcarriers are represented by 2N bits, and in QPSK modulation there are 2^{2N} messages. The whole message space corresponds to zero bits of redundancy, half of the messages correspond to one bit of redundancy, the remaining message space is divided in half again. This process continues until all N bits of redundancy have been allocated. Figure 5-7 is the PAPR for up to 15 carriers for different bits of redundancy (note: in the graph, the maximum PAPR is set to N instead of 2N).

MAXIMUM PEP USING REDUNDANCY (Kb)

K	Number of carriers													
	2	3	4	5	6	7	8	9	10	11	12	13	14	15
0	**2.00**	**3.00**	4.00	5.00	6.00	7.00	8.00	9.00	10.00	11.00	12.00	13.00	14.00	15.00
1	2.00	2.61	**2.57**	**2.79**	3.03	3.26	3.30	3.42	3.57	3.67	3.73	3.82	3.89	3.97
2	2.00	1.67	2.00	2.24	**2.71**	**2.67**	**2.82**	**2.95**	3.06	3.11	3.19	3.27	3.34	3.39
3	-	1.67	1.77	2.11	2.39	2.53	2.64	2.78	**2.84**	**2.91**	3.01	3.08	3.13	3.19
4	-	-	1.77	2.10	2.27	2.44	2.56	2.67	2.73	2.80	**2.91**	**2.96**	3.01	3.07
5	-	-	-	2.09	2.22	2.43	2.51	2.61	2.67	2.73	2.85	2.89	**2.93**	**3.00**
6	-	-	-	-	2.20	2.38	2.48	2.56	2.63	2.68	2.80	2.85	2.88	2.95
7	-	-	-	-	-	2.36	2.43	2.52	2.60	2.65	2.74	2.80	2.85	2.90
8	-	-	-	-	-	-	2.40	2.49	2.57	2.62	2.70	2.76	2.81	2.86
9	-	-	-	-	-	-	-	2.46	2.53	2.59	2.67	2.72	2.78	2.84
10	-	-	-	-	-	-	-	-	2.50	2.57	2.64	2.69	2.75	2.81
11	-	-	-	-	-	-	-	-	-	2.52	2.62	2.67	2.73	2.79
12	-	-	-	-	-	-	-	-	-	-	2.59	2.65	2.70	2.77
13	-	-	-	-	-	-	-	-	-	-	-	2.64	2.69	2.75
14	-	-	-	-	-	-	-	-	-	-	-	-	2.69	2.73
15	-	-	-	-	-	-	-	-	-	-	-	-	-	2.71

Figure 5-7 Maxmum PEP Using Redundancy [24]

In Figure 5-7, we see thePAPR reduced down to 4 and below for up to 15 carriers with one bit of redundancy. And with just a few more bits of redundancy, we can keep the PAPR below 3. As the number of carriers increases, the amount of redundancy needed to achieve a PAPR of below 3 converges toward a rate ¾ code [24].

5.1.2.3 Clipping and Filtering

Coding does not introduce any distortion to the signal. However, as the number of carriers increases, coding becomes intractable since the memory needed to store the codebook and the CPU time needed to find the corresponding codeword grows exponentially with the number of carriers. Clipping causes significant spectral leak into adjacent channels (Figure 5-5).

Out-of-band components cause adjacent channel interference. Filtering can be applied to reduce the interference. But the act of filtering causes peak re-growth. Figure 5-5 is the result of clipping without filtering. Figure 5-8 is the result of filtered 128-carrier OFDM signal [32]. After filtering, the out-of-band interference is suppressed. But filtering causes peak regrowth (see Figure 5-9 and Figure 5-10). Most peak regrowth is about 4 to 5 dB. But amplitudes are concentrated at lower levels. Despite the peak regrowth, filtering is effective.

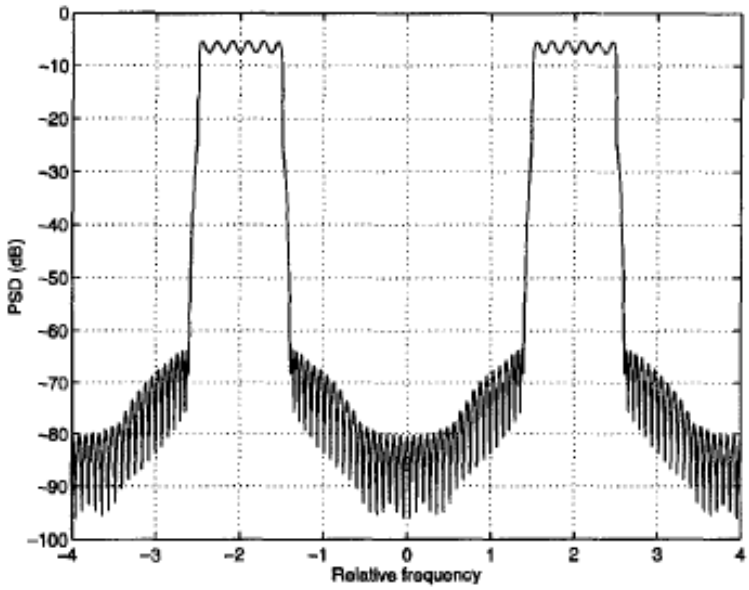

Figure 5-8 PSD of the Clipped and Filtered Signal CR = 1.4

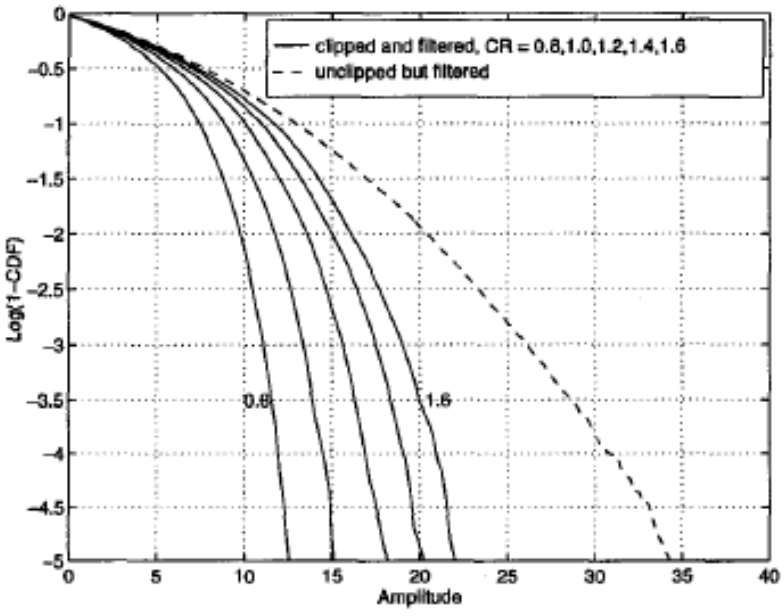

Figure 5-9 Log (1-CDF) Function of the Amplitude of the Clipped Signal

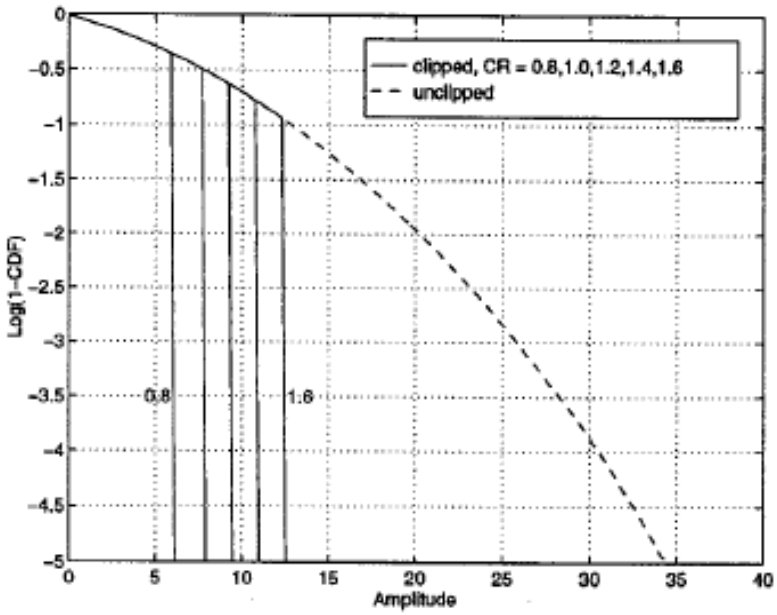

Figure 5-10 Log (1-CDF) Function of the Amplitude of the Clipped and Ciltered Signal

The in-band interference introduces additional noise because the information contained in the clipped portion is lost. This can be modeled as a white Gausian noise if several events of clipping occur within an OFDM symbol. By the reduced quantization noise of the A/D-D/A converters, the additional noise can be compensated. This is because of a reduction in their dynamical ranges. The signal-to-clipping noise power ratio is given by equation 5.3 [33].

$$(S/N)_{Clip} = ((1+\mu^2).erfc(\frac{\mu}{\sqrt{2}}.\mu.e^{-\frac{\mu^2}{2}}))^{-1} \tag{5.3}$$

where μ is the same as the clipping ratio (CR) defined above.

Based on the assumption that the noise caused by clipping can be modeled by a white Guassian noise we can analyze the clipping noise. Clipping noise is modeled as an impulsive noise to better describe the noise. The resulting performance can be orders of magnitude worse than the performance obtained by the white noise model [36]. From equation 5.4, the number of bits needed by the A/D to quantize the signal after clipping can be determined. For N = 256 and

A_{Clip}= (A_{max} / 6), the number of bits of the A/D-D/A can be decreased by more than 2 to achieve the same performance as if clipping was not applied [33].

$$(S/N)_{Q1}^{-1} = (S/N)_{Q2}^{-1} + (S/N)_{Clip}^{-1} \tag{5.4}$$

where $(S / N)_{Q1}$ is the signal-to-quantization noise ratio without clipping and $(S / N)_{Q2}$ is the signal-to-quantization noise ratio after clipping.

5.2 Carrier Phase Tracking

There is always some residual frequency error even after frequency estimation. The SNR loss due to the inter-carrier interference (ICI) generated does not affect the performance if the estimator has been designed to reduce the frequency error below the limit required for a negligible performance loss for the used modulation. The main problem of the residual frequency offset is constellation rotation. Figure 5-11 shows how much IEEE 802.11a QPSK constellation rotates during 10 OFDM symbols with a 3kHz frequency error. It is found that the constellation rotation is the same for all subcarriers. This error corresponds to only 1% of the subcarrier spacing, thus the effect on SNR is negligible [31].

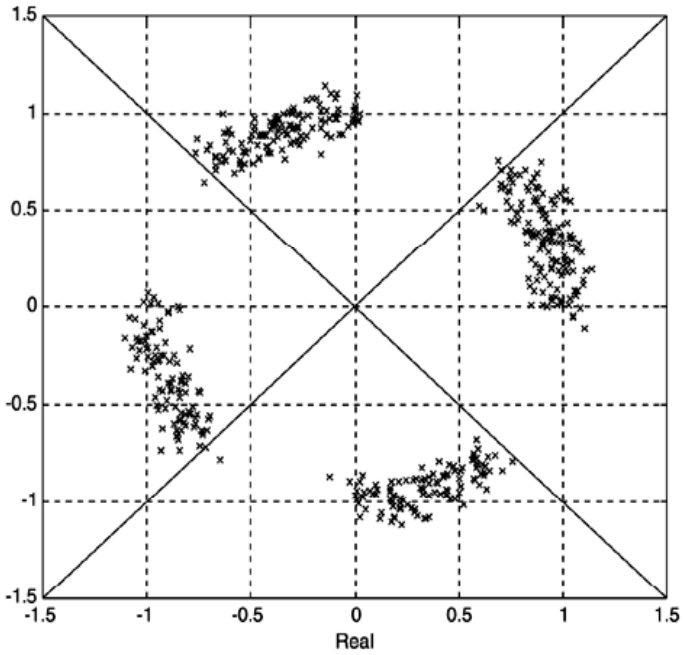

Figure 5-11 Constellation Rotation with Frequency Error [31]

Figure 5-11 shows that after only 10 symbols, the constellation points have just rotated over the decision boundaries shown as solid lines, thus correct demodulation is no longer possible. This effect forces the receiver to track the carrier phase while data symbols are received.

Most commonly used method is data-aided tracking of the carrier phase. UWB OFDM has 12 special subcarriers referred to as *pilot* subcarriers. The pilots are designed to help the receiver to track the carrier phase. After the DFT of the *n*th received symbol, the pilot subcarriers R_{nk} are equal to the product of the channel frequency response H_k and the known pilot symbol P_{nk}, rotated by the residual frequency error (See equation 5.5). Assuming an estimate $\hat{H}_k$ of the channel frequency response is available, the phase estimate is shown in equation 5.6. Assume that the channel estimate is perfectly accurate, we can get the estimator as in equation 5.7 [31].

$$R_{nk} = H_k P_{nk} e^{j2\pi n f_\Delta} \tag{5.5}$$

$$\hat{\Phi}_{nk} = \angle\left[\sum_{k=1}^{N_p} R_{n,k}(\hat{H}_k P_{nk})\right] \tag{5.6}$$

$$\hat{\Phi}_n = \angle\left[e^{j2\pi n f_\Delta} \sum_{k=1}^{N_p} \left|\hat{H}_k\right|^2\right] \tag{5.7}$$

The pilot data is predefined, so the phase ambiguity is automatically resolved correctly. Because in practice the channel estimates are not perfectly accurate, thus they contribute to the noise in the estimate.

Chapter 6 Radio on Fiber System Design and Simulation

In this chapter, we provide simulation and design based the theory and analysis from Chapter 4 and Chapter 5. This chapter consists of three sections: optical system design and simulation, UWB system design and simulation, integration simulation of optical and wireless RoF system. The software connector is implemented interconnect Rsoft Optsim and Matlab Simulink.

6.1 Optical System Design and Simulation

This section presents VCSEL optical system design. Because of limited time and lab facility, simulation using industrial design and simulation suit Optsim from Rsoft Design Group is carried out instead of lab testing. VCSEL dynamics prosperities are simulated for single mode and multimode fiber at different bias currencies. The design and simulation meant to provide design guidelines VCSEL optical system for UWB wideband Radio on Fiber.

6.1.1 Simulation Setup

The optical system design consists of VCSEL diode transmitter, single/multimode fiber, attenuator, PIN diode receiver. Optsim 4.0 optical simulation tool from Rsoft Design Group is used for the design. Figure 6-1 shows the VCSEL optical system design. UWB RF signal is fed in to the optical system through a test data file reader block. Electrical and optical spectrum analyzers are attached to the input and output electrical and optical signals. Test data file writer collects electrical system after optical transmission for simulation in Matlab Simulink (Figure 6-13).

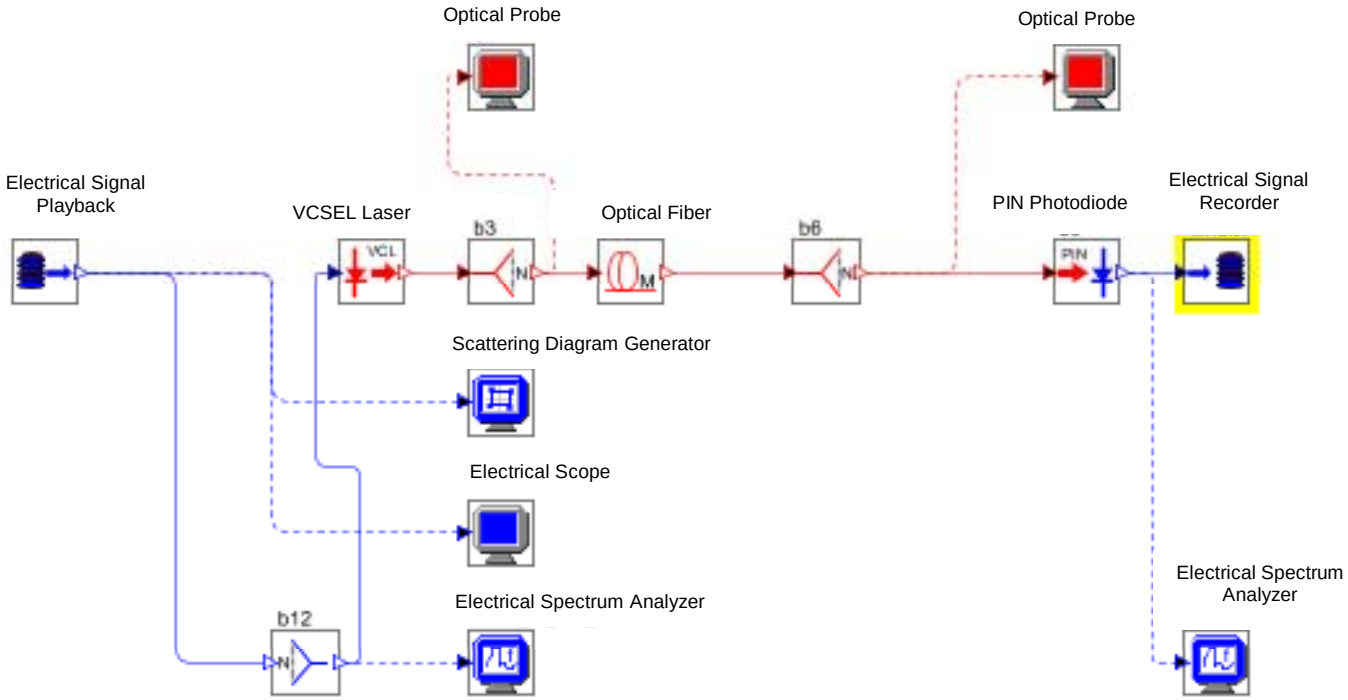

Figure 6-1 VCSEL Optical System Design Using Optsim Design Suite

All the parameters for the simulation are taken from commercial products. Honeywell HFE4080-32X/XBA VCSEL is used as laser emitter (Table 6-1). Corning SMF-28 is used as single mode fiber (Table 6-2). Corning Infinicor 1000 is used as multimode fiber (Table 6-3).

Table 6-1 VCSEL Laser Emitter

Honeywell VCSEL Laser Emitter
Honeywell High Speed Fiber Optic VCSEL (HFE4080-32X/XBA)
Threshold current I_{TH} 3.5 mA
Slope Efficiency η 0.3 mW/mA
Peak Wavelength λ_P 820 850 860 nm
Spectral Bandwidth $\Delta\lambda$ 0.5 nm

Table 6-2 Single Mode Fiber

Corning SMF-28
850 nm LED source minimum overfilled launch bandwidth 200 MHz * km
Laser based source 385 MHz* km
Attenuation: < 0.35/0.22 dB/km @ 1310/1350 nm
Chromatic Dispersion:
Zero Dispersion Wavelength (λ_0) 1302 nm $\leq \lambda_0 \leq$ 1322 nm
Zero Dispersio Slope (S_0) $\leq$ 0.092 ps/(nm^2 *km)
Dispersion = D(λ) = $S_0 \frac{S_0}{4}\left[\lambda - \frac{\lambda_0^4}{\lambda^3}\right]$ ps/(nm*km)
Mode-Field Diameter:
$9.2 \pm 0.4 \mu m$ at 1210 nm, $10.4 \pm 0.8 \mu m$ at 1550 nm
Length: 0.5 km

Table 6-3 Multimode Fiber

Corning Infinicor 1000 multimode fiber
850 nm LED source minimum overfilled launch bandwidth 200 MHz * km
Laser based source 385 MHz* km
Attenuation: < 3.0/0.7 dB/km @ 850/1300 nm
Chromatic Dispersion:
Zero Dispersion Wavelength (λ_0) 1332 nm $\leq \lambda_0 \leq$ 1354 nm
Zero Dispersio Slope (S_0) $\leq$ 0.0097 ps/(nm^2*km)
Dispersion = D(λ) = $S_0 \frac{S_0}{4}\left[\lambda - \frac{\lambda_0^4}{\lambda^3}\right]$ ps/(nm*km)
Core Diameter: 63.5 +/- μm
Numerical Aperture: 0.275 +/- 0.015
Length: 0.5 km

6.1.2 VCSEL Optical Simulation

This section presents the simulation of VCSEL transmits in single and multimode fiber. Oxide aperture diameter of 2 μm is simulated for single mode and oxide aperture diameter of 10 μm is simulated for multimode.

6.1.2.1 Output Power Response

The single mode power versus current characteristics is shown in Figure 6-2. The multi mode power versus current characteristics is shown in Figure 6-3. We can see that, the 2μm single-mode VCSEL has better slope efficiency than the 10μm multimode VCSEL (0.2 versus 0.35 W A^{-1}), and lower maximum power (0.9 versus 4 mW).

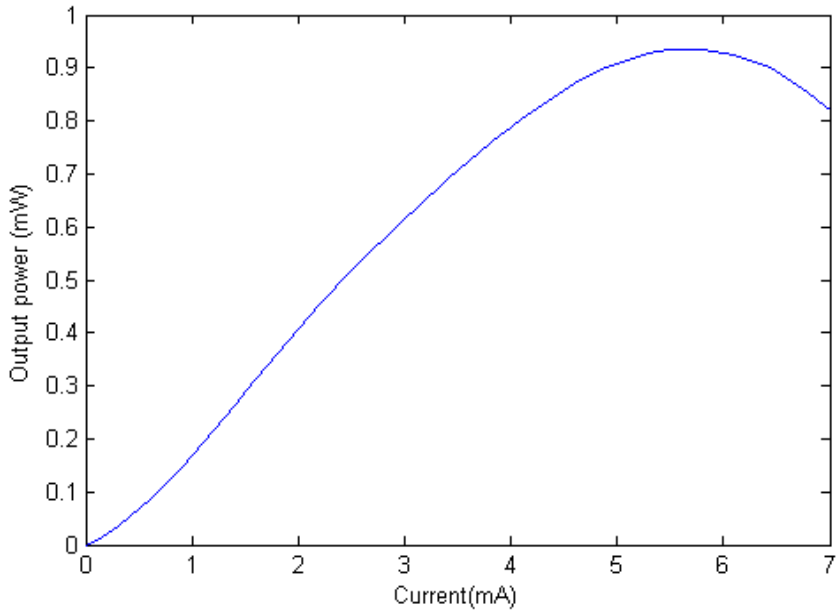

Figure 6-2 Output Power vs. Current for 2 μm Single Mode VCSEL

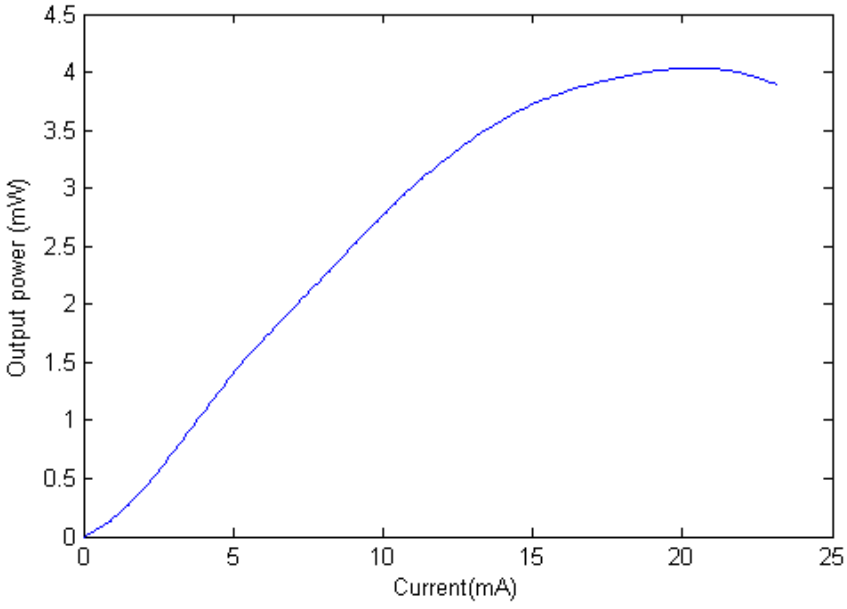

Figure 6-3 Output Power for 10 μm Multimode VCSEL

6.1.2.2 Modulation Response and Bandwidth

Single mode and multi mode small signal modulation at difference bias currents are simulated and shown in Figure 6-4 and Figure 6-5 respectively. Performing the analysis from section 4.1.2, we find that the modulation bandwidth of the 10μm multimode VCSEL is limited to 12 GHz at 8 mA by a combination of damping and parasitic effects. From the same analysis see can see that, the modulation bandwidth of the 2μm single-mode VCSEL is limited to 9 GHz at 2 mA by a considerably higher damping due to strong gain compression. This is the result of the high photon density.

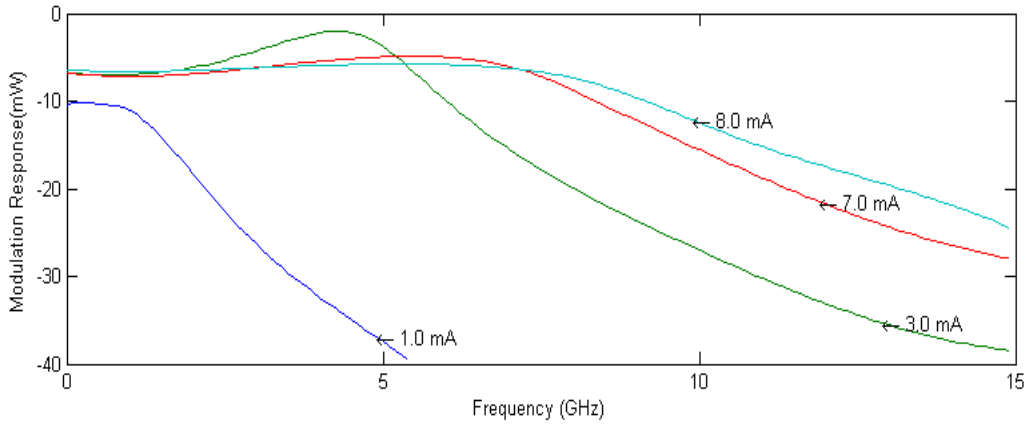

Figure 6-4 Small Signal Modulation Response for 2µm single Mode VCSEL at Different Bias Currents

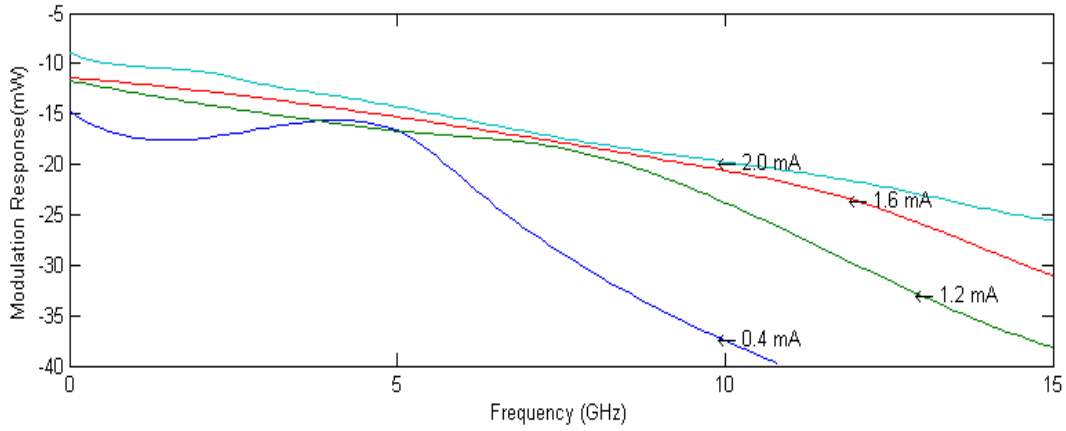

Figure 6-5 Small Signal Modulation Response for 10μm Multi Mode VCSEL at Different Bias Currents

Performing the D-factor analysis from section 4.1.2, we find that the 10μm multimode VCSEL has a *D*-factor of 4.2 GHz $mA^{-1/2}$. However performing the same analysis the 2μm single-mode VCSEL has a *D*-factor of 11.5 GHz $mA^{-1/2}$. The high value of the *D*-factor for the single-mode VCSEL is a result of the small cavity and gain volumes and the high photon density.

Multimode VCSEL has a modulation response at frequencies below the resonance frequency, which is about 10–15 dB higher. This is due to the lower parasitic RF loss and also due to the higher slope efficiency. In this case, single-mode VCSEL is favored by a high *D*-factor.

6.1.2.3 Relative Intensity Noise (RIN)

RIN is analyzed in section 4.1.4. Simulation is carried out for single and multi mode VCSEL at different bias currents. Figure 6-6 shows RIN spectra for VCSELs at different bias currents for 2μm single mode. Figure 6-7 shows RIN spectra for VCSELs at different bias currents for 10μm multi mode.

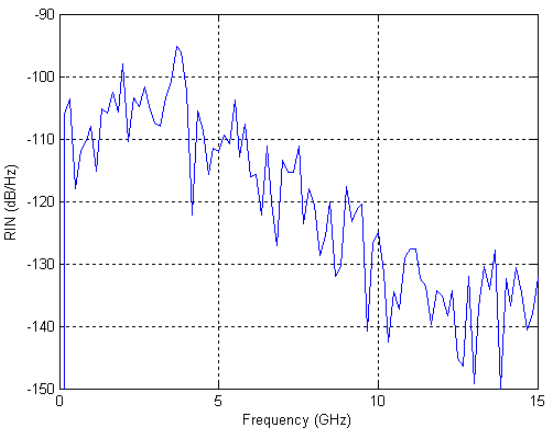

a) 0.8 mA

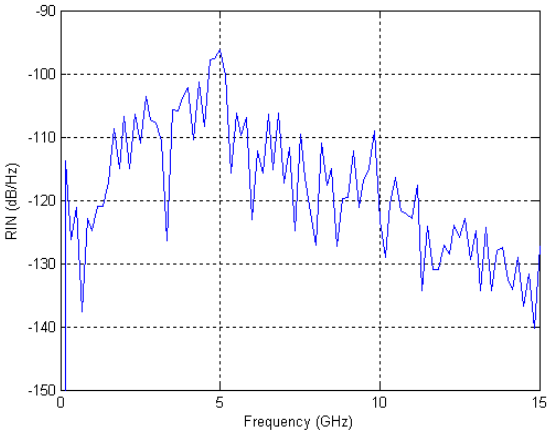

b) 1.2 mA

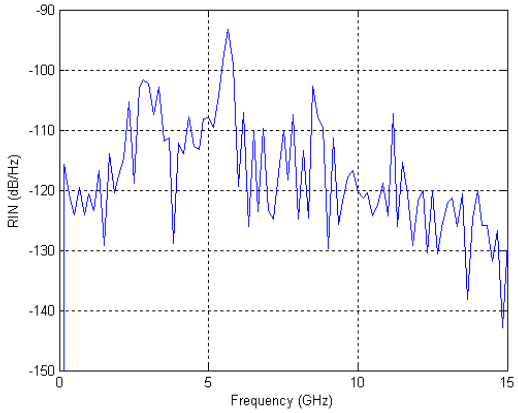

c) 2.0 mA

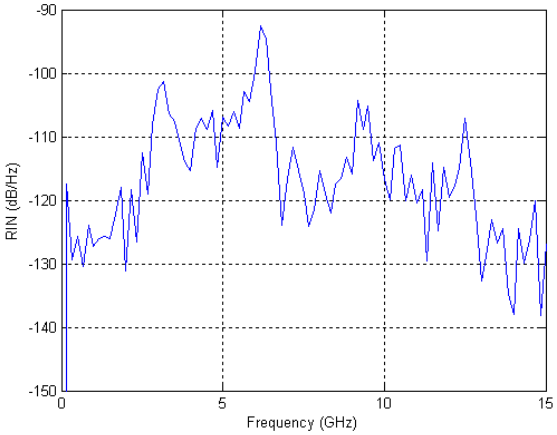

d) 3.0 mA

Figure 6-6 RIN Rpectra for 2μm Single Mode VCSELs at Different Bias Currents

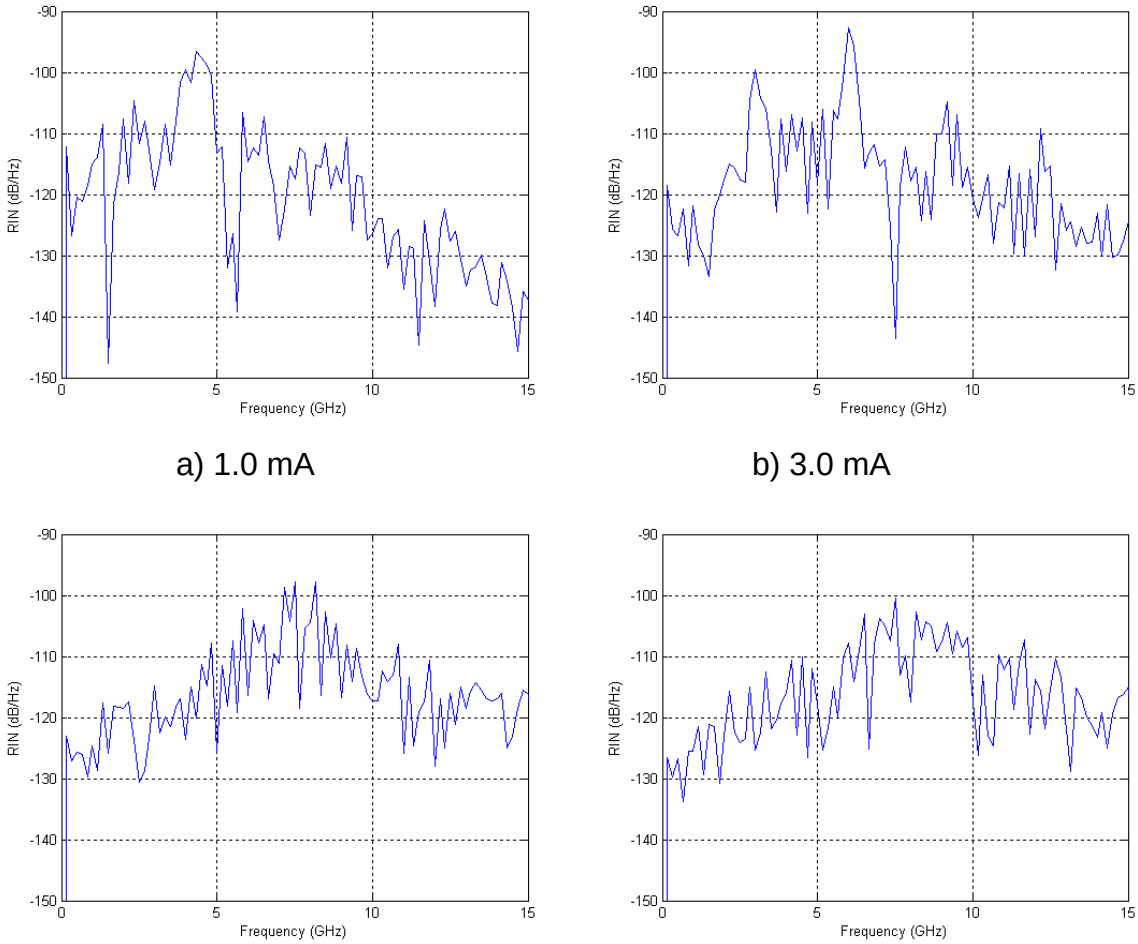

a) 1.0 mA

b) 3.0 mA

c) 5.0 mA

d) 8.0 mA

Figure 6-7 RIN Spectra for 10μm Multi Mode VCSELs at Different Bias Currents

We can see from the simulation, at high bias current, the noise of the single-mode VCSEL saturates at the shot noise floor. However the noise of the multimode VCSEL is higher due to mode competition or mode partition noise, and because of unavoidable mode-selective coupling. So we can see that single-mode is more favorable because the single-mode VCSEL has the lowest intensity noise.

6.1.2.4 Dynamic Range

Second order harmonic distortion of signal and multimode VCSEL at different bias currents are simulated. Figure 6-8 shows single mode VCSEL second order harmonic distortion. Figure 6-9 shows multi mode VCSEL second order harmonic distortion. At lower frequencies (<1.5 GHz for single mode, < 2.0 GHz for multi mode), spatial hole-burning-induced distortion dominates. At intermediate frequencies, the two effects from relaxation oscillation and spatial hole burning cancel each other, resulting in a significantly lower distortion. Spectral hole burning effect, which is accounted for by the gain compression factor were found to have a small effect on the relative distortion levels.

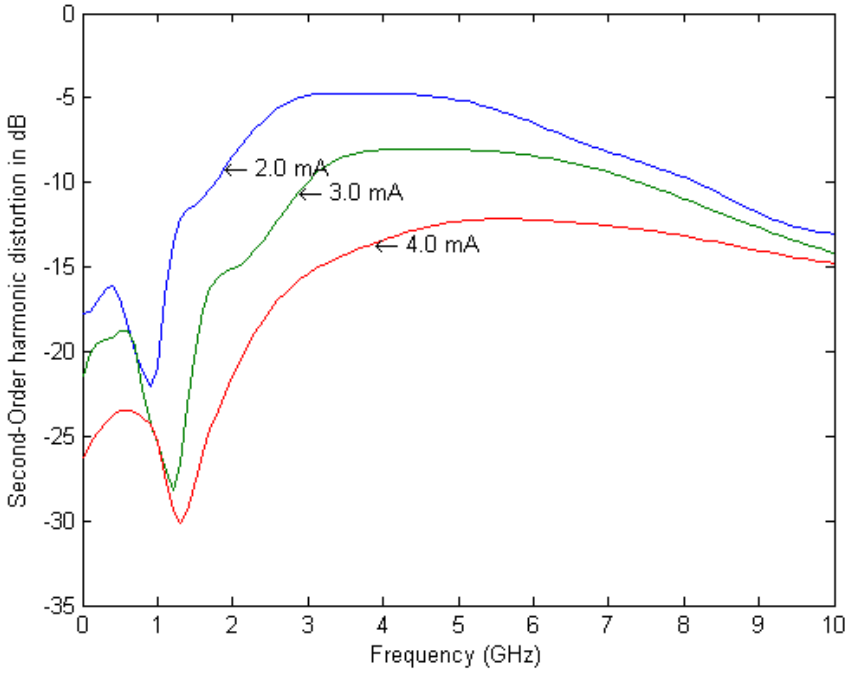

Figure 6-8 Single Mode VCSEL Second Order Harmonic Distortion

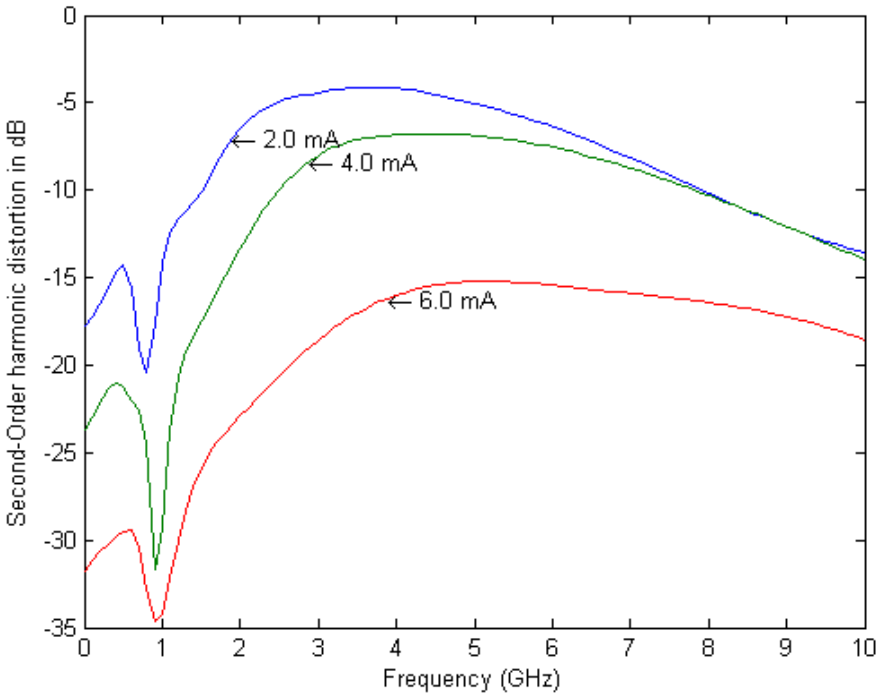

Figure 6-9 Multi Mode VCSEL Second Order Harmonic Distortion

Spurious Free Dynamic Range (SFDR) is calculated from two-tone inter-modulation distortion (IMD) simulation. Two-tone signal separated in frequency by 1 MHz was fed to VCSEL with different bias current. See Figure 6-10 for the setup of SFDR simulation. The simulation results are shown in Figure 6-11 from single mode and Figure 6-12 for multimode VCSEL. The SFDR of the multimode VCSEL at 6 mA bias current is 84-95 dB. And the SFDR of the single mode VCSEL at 2 mA bias current is 82-85 dB. The SFDR of Single mode VCSEL is about 10 dB lower than multimode VCSEL. This is because of lower modulation response of the single mode VCSEL. We can see that RF transfer efficiency of multimode is greater than single mode VCSEL.

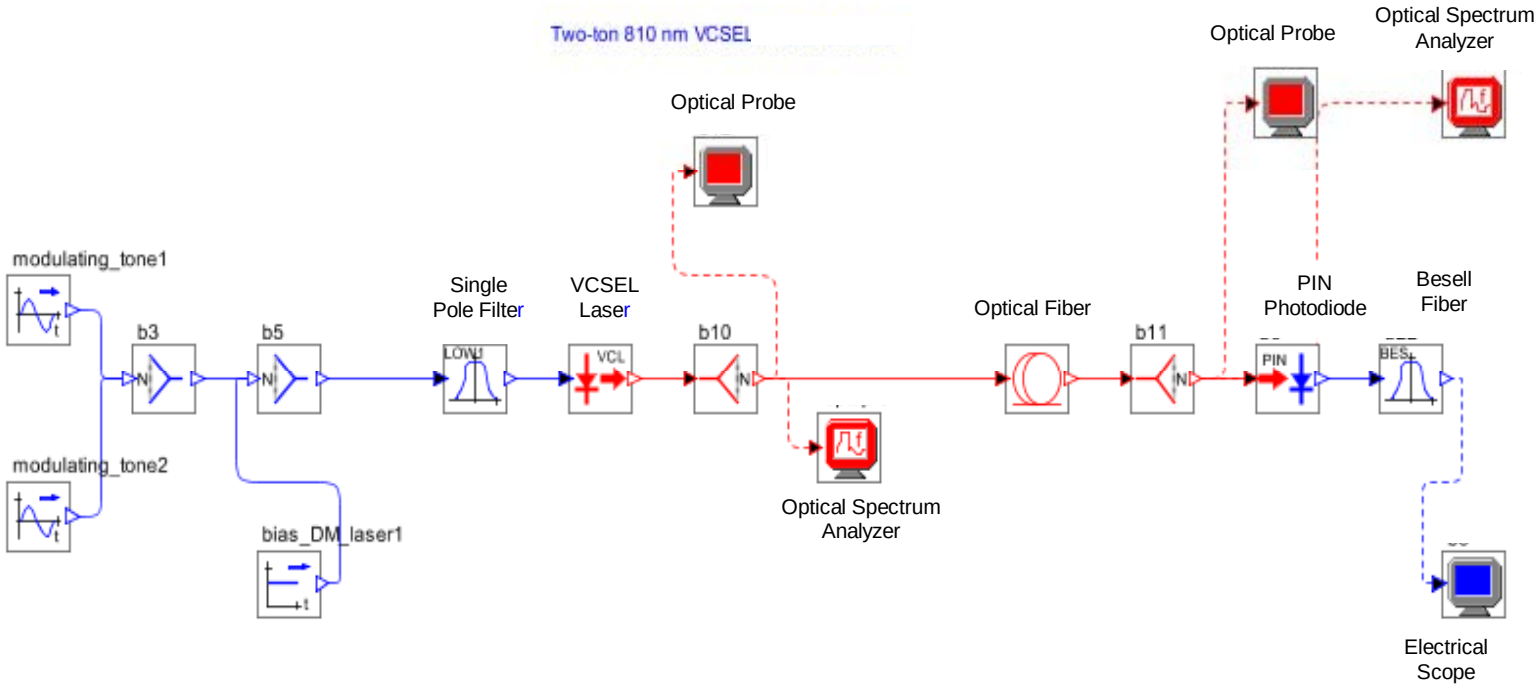

Figure 6-10 Optsim Design for Two-ton Test

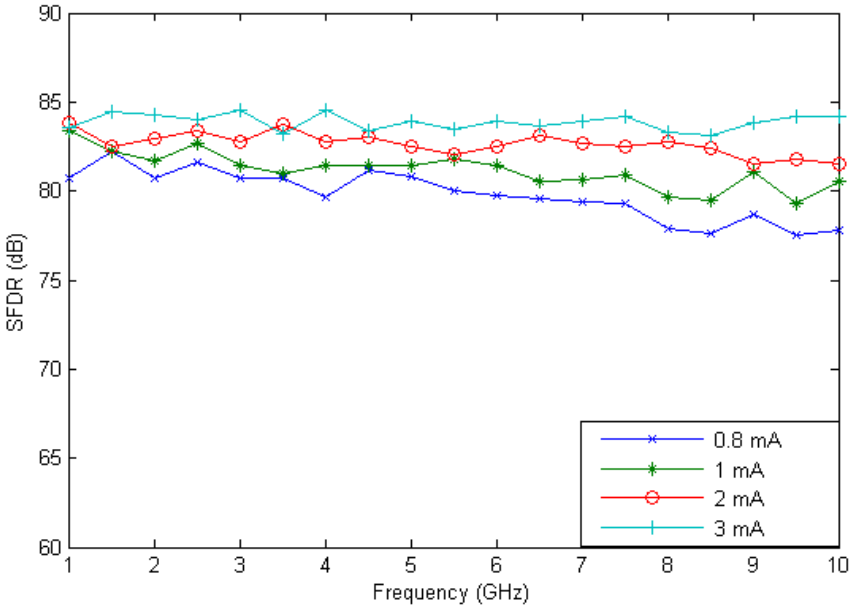

Figure 6-11 SFDR for 2mm Single Mode VCSEL

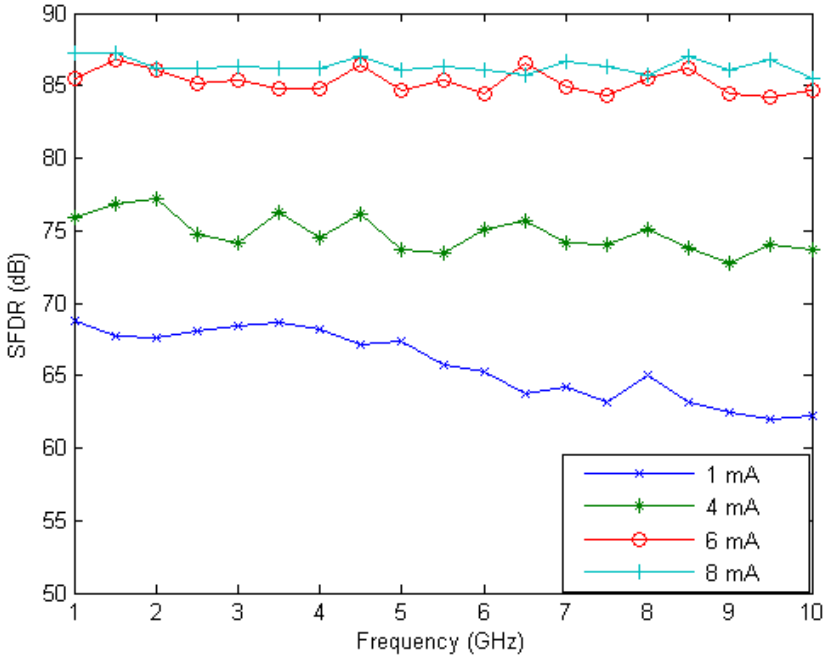

Figure 6-12 SFDR for 10 mm Multi Mode VCSEL

6.1.3 Optical System Summary

Desirable characteristics of a VCSEL (or any laser) used in a directly modulated fiber optic RF link include:

- Small parasitic RF loss.
- Low relative intensity noise (RIN)
- Low distortion
- High fiber-coupling efficiency

Low RIN levels and high coupling efficiency suggest the use of a single mode VCSEL. Because single mode VCSEL has no mode partition noise and low beam divergence. Major sources of distortion are the intrinsic non-linearity associated with the relaxation oscillations and spatial hole-burning-induced distortion[45]. From the above it shows that the performance under direct high frequency modulation should depend on the modal characteristics of the VCSEL. VCSEL has a high resonance frequency and a strongly clamped carrier density because of the high photon density. So the use of a single mode VCSEL is more favorable over multimode VCSEL in analog signal transmission.

From simulation under different bias currencies we found: For single mode VCSEL, the bias of 2 mA has the highest SFDR and low RIN. For multimode VCSEL, the bias of 6 mA has the highest SFDR and low RIN. Since single mode VCSEL is more favorable in analog signal transmission, we chose single mode VCSEL with bias of 2 mA as optical link in the UWB RoF system.

6.2 UWB System Design and Simulation

This section presents UWB design of RoF system. The design is simulated using Matlab Simulink (Figure 6-13). The Simulink design is based on IEEE 802.15.3a proposal. Optical simulation is carried on through VCSEL Optical Channel block, which communicates to Rsoft optical design/simulation suite. Our design based on Matlab 802.15 model and testing data from IEEE 802.3z Gigabit Ethernet Standard Effort. The software connector sends UWB RF signal data generated from Simulink to Rsoft Optsim for optical simulation. UWB RF signal distributed through optical simulation is sent back to Simulink. "VCSEL Optical Channel" block in Figure 6-13 is software connector that provides the link between the two simulation systems.

UWB OFDM signal has large number of carriers, and the most effective method to mitigate PAPR is through clipping and filtering. In this section clipping based PAPR method optimized for UWB OFDM is proposed. Analysis and simulation are carried out.

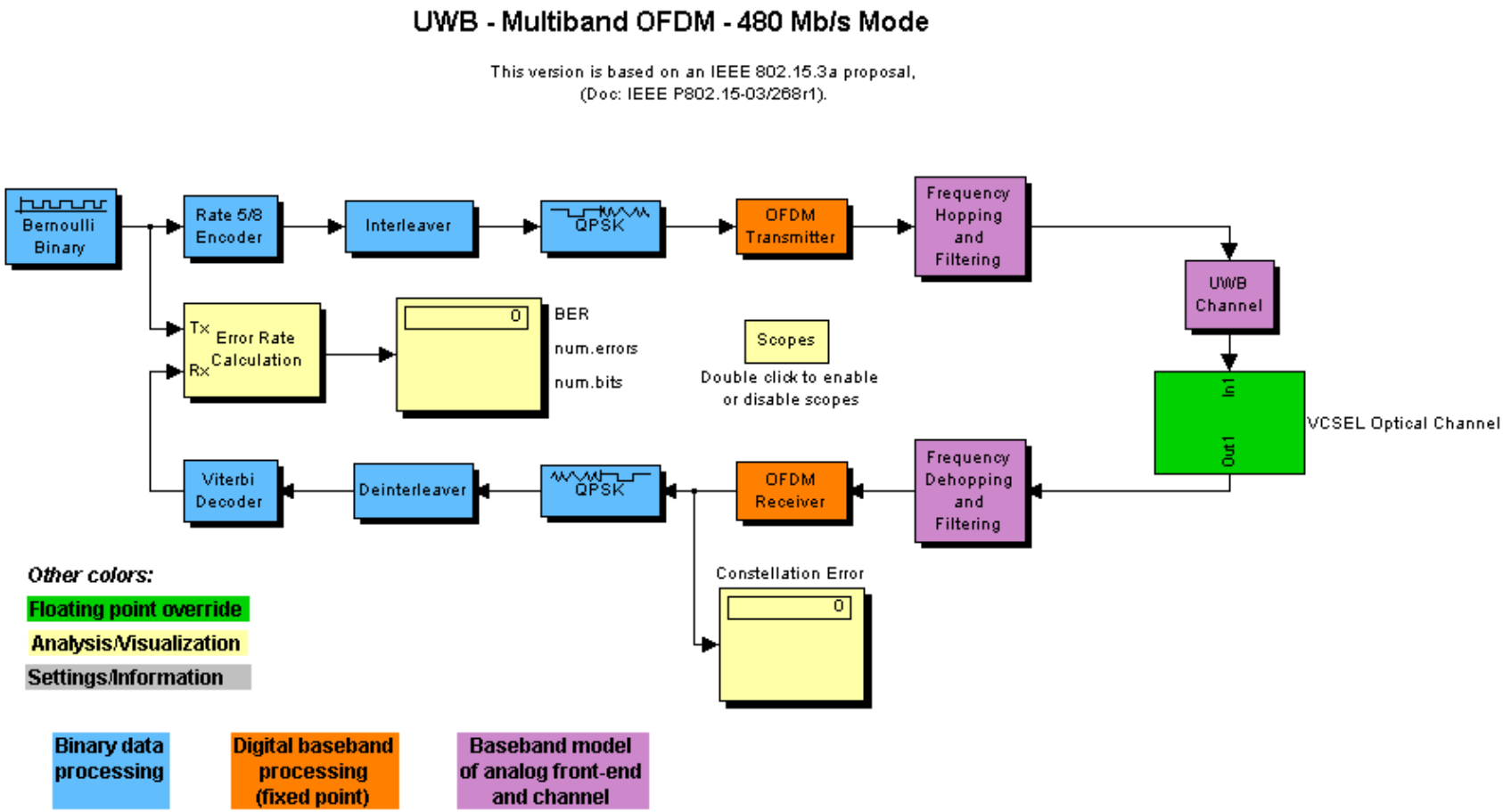

Figure 6-13 480 Mb/s UWB Design Using Matlab Simulink

6.2.1 Signal Over Sampling and Envelope Clipping

From discussion in previous sections, we see that occurrence of high PAPR is very low. Clipping of UWB OFDM signal baseband envelope is a very effective method in reducing PAPR, because UWB signal has big number of subcarriers. This is because the efficiency does not depend on the number of subcarriers, which fits well for UWB signals. Because in-band clipping noise of UWB OFDM signals cannot be reduced by filtering, we use over sampling of UWB OFDM signal to address the aliasing problem. Figure 6-14 shows the complex envelope of over sampled baseband UWB OFDM signal. UWB OFDM signal possesses random high-energy peaks shown in the figure. We can see that high-energy peaks are generated when subcarriers add constructively. The clipping threshold is chosen to be set above the root mean square (RMS) signal power level. Figure 6-15 shows corresponding baseband envelope clipped signal. After clipping, high-energy random peaks have been removed. The clipping threshold A is defined in equation 6.1. The equation defines the over sampled complex baseband UWB OFDM signal.

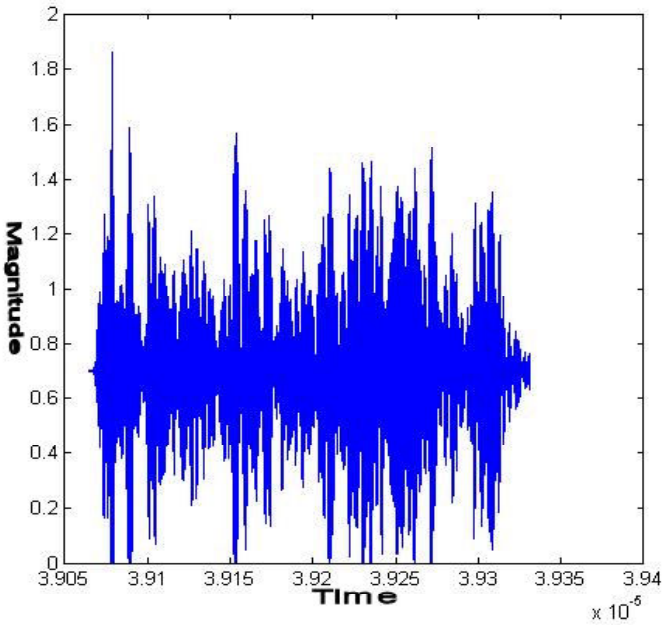

Figure 6-14 Complex Envelope of Baseband OFDM Signal

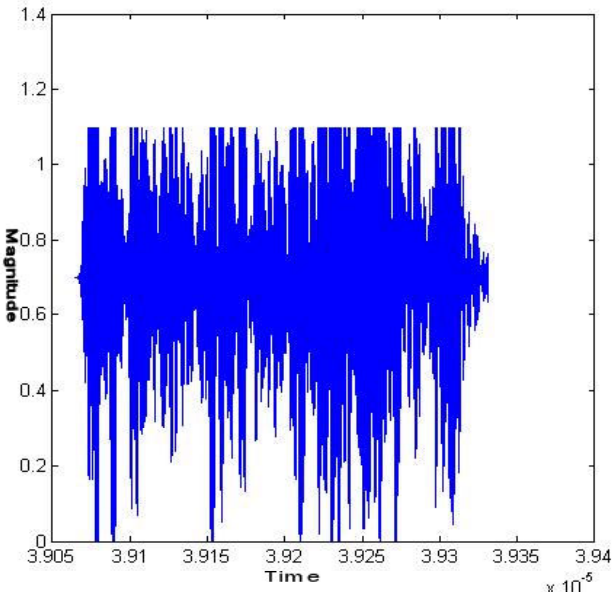

Figure 6-15 Complex Envelope of Baseband Clicpped OFDM Signal

$$A = 10^{\frac{CR}{20}} \frac{\|S_t\|}{\sqrt{N}} \tag{6.1}$$

where S_t is the over sampled base band OFDM signal, CR is clipping ratio and N is the number of subcarriers.

Equation 6.2 defines the clipped complex envelope of the baseband UWB OFDM signal. This is the conventional method for clipping, which performs a complex envelope clipping of the baseband UWB OFDM signal.

$$S_t = \begin{cases} S_t & |S_t| \le A \\ A \angle S_t & |S_t| \ge A \end{cases} \tag{6.2}$$

The clipping operation does not alter phase information. After complex envelope clipping of the baseband OFDM signal, the signal PAPR reduces greatly. Figure 6-16 shows the PAPR of the original and clipped signal.

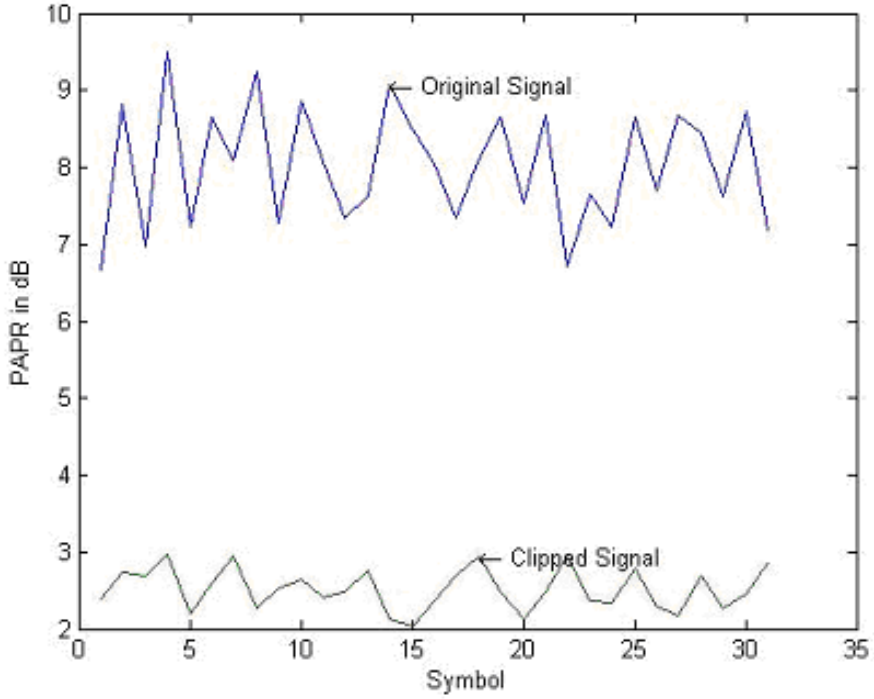

Figure 6-16 PAPR of Clipped and Original Signal (Clipping Threshold = 3dB)

From the discussion in the previous section, reduction of PAPR is highly desirable for OFDM signal transmission over fiber optic channel to mitigate nonlinear distortion. Low PAPR means low modulation index and subsequently less non-linear effects on VCSEL diode. The conventional clipping process reduced PAPR but also generates in-band and out of band clipping noise. This is showed in equation 6.3.

$$\widetilde{S}_t = S_t + C_t^{In} + C_t^{Out} \tag{6.3}$$

where is the original signal, is in band clipping noise, is out of band clipping noise and is the original signal plus the clipping noise.

Clipping causes significant out of band and in band clipping noise. Out of band clipping noise is caused by spectral leakage into adjacent channels. Clipping Threshold is 3dB above the RMS signal Power, the spectrum of clipped and original signal is shown in Figure 6-17. However in band clipping noise cannot be clearly shown in the figure. BER and RMS constellation error can be used to evaluate in band clipping noise.

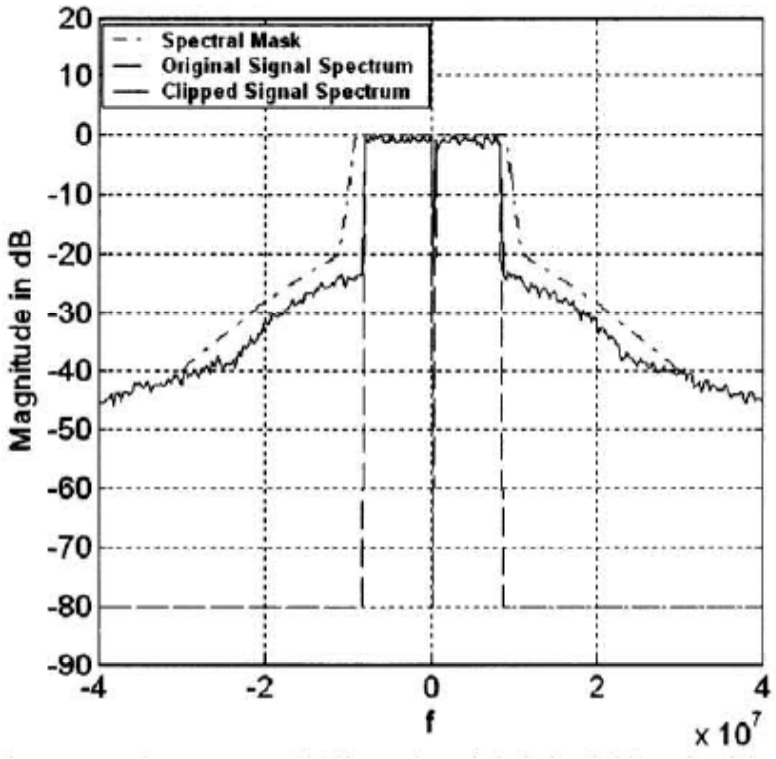

Figure 6-17 Spectrum of Clipped and Original Signal

The premise of the clipping process is multiplying the original signal with a threshold. The peaks are above the clipping threshold. The peaks then are replaced by the threshold (See equation 6.2). The original signal spectrum is convolved in frequency domain with the spectrum

of the clipping function. P is defined as the number of clipped peaks over the symbol interval; the original signal spectrum is convolved with the spectrum of clipping function P times. This is shown in equation 6.4.

$$\widetilde{S}_f = S_f * (D_f * ... * D_f)_{1xP} \tag{6.4}$$

where S_f is the original signal in frequency domain, $\widetilde{S}_f$ is the clipped signal in frequency domain , and D_f is spectrum of clipping threshold and P is the number of peaks clipped over the symbol interval.

For the rectangular window using a threshold, the clipped peak spectrum is a sinc function. The subcarrier magnitudes of S_f are distorted by the repeated convolution of D_f with S_f. The distortion effect depends on the spectral width of D_f. When the spectral width of D_f reduces to become comparable to the subcarrier separation of S_f, the subcarrier magnitude distortion reduces due to the convolution process. With the increase of spectral width of D_f, adjacent subcarriers have more effect on the magnitude of present subcarrier, as a result distorts the magnitude.

Baseband over sampling is performed through zero padding of mapped data during the OFDM baseband signal generation process to minimize the above effect introduced. Due to baseband over sampling, peaks are also over sampled. That means each peak now has a width which in turn reduces the spectral width of D_f and consequently generates less in-band clipping noise after going through clipping process as discussed above.

We can say from the above discussion that clipping of over sampled baseband envelope is an effective method to reduce signal dynamic range and consequently non-linear distortion due to electro-optic modulator. On the other hand, clipping process introduces noise to the original

signal and affects system performances. In-band clipping noise is reduced through over sampling of baseband OFDM signal. However out of band clipping noise has to be handled separately.

6.2.2 Signal Peak Windowing

Applying windowing to the clipped peak can reduce out-of-band noise. This process will remove the sharp edges of the clipped peak and subsequently reduce spectral leakage. In this thesis this over sampled clipping and windowing process is named Window-Clipping. A few window functions were investigated: Gaussian, Tukey, Chebyshev, Prolate, Spheroidal and Kaiser. Each window has its unique characteristic. We need to find the optimal window that can lower PAPR and keep the performance loss to a minimum amount. equation 6.5 describes the new clipping process in time domain and equation 6.6 in frequency domain. From the discussion above, the original signal spectrum S_t is convolved with the spectrum of window function W_f P times after the window-clipping process.

$$S_t = \begin{cases} S_t & |S_t| \le A \\ W_t \angle S_t & |S_t \ge A| \end{cases} \tag{6.5}$$

where W_t is the real valued window function

$$\widetilde{S}_f = S_f * (W_f * \ldots * W_f)_{1xP} \tag{6.6}$$

where W_f is the real valued window function P is the number of peaks clipped over the symbol interval.

The side lobe attenuation of W_f is better than the rectangular window D_f, the new clipping process reduces out of band clipping noise. Each of the window functions has its pros and cons. The type of the window function and the parameter of the window have great impact on the performance of the new clipping method. The window function used in window clipping should

have optimum main lobe width (comparable to the subcarrier spacing in the UWB OFDM symbols) and maximum side lobe attenuation. The objective is to find the optimum window function and window parameters of the window function so that it generates minimum amount of in-band as well as out-of-band clipping noise using an iterative method. Analysis and simulation are carried out for the window functions for UWB OFDM signal. Among all window functions under study, Kaiser window has minimum main lobe width and maximum side lobe attenuation, there for it is the most favorable window function.

With the same over sampling ratio, the spectral width of window function W_f is more than the spectral width of rectangular window D_f. That is why repeated convolution of W_f with S_f distorts subcarrier magnitudes of S_f more than similar repeated convolution of D_f with S_f. As a result, window-clipping process increases in band clipping noise. However, due to higher side lobe attenuation of W_f compare to D_f, window-clipping has better performance to reduce out of band clipping noise. Figure 6-18 shows the spectrum of original base band UWB OFDM signal, Figure 6-19 shows the spectrum of clipped signal with clipping threshold 3 dB. Figure 6-20 shows the spectrum of clipped signal with 3 dB clipping and window function is Kaiser 3.6. From Figure 6-18, Figure 6-19 and Figure 6-20 we can observe that window clipping generates less out of band noise compared to only over sampled-clipping process.

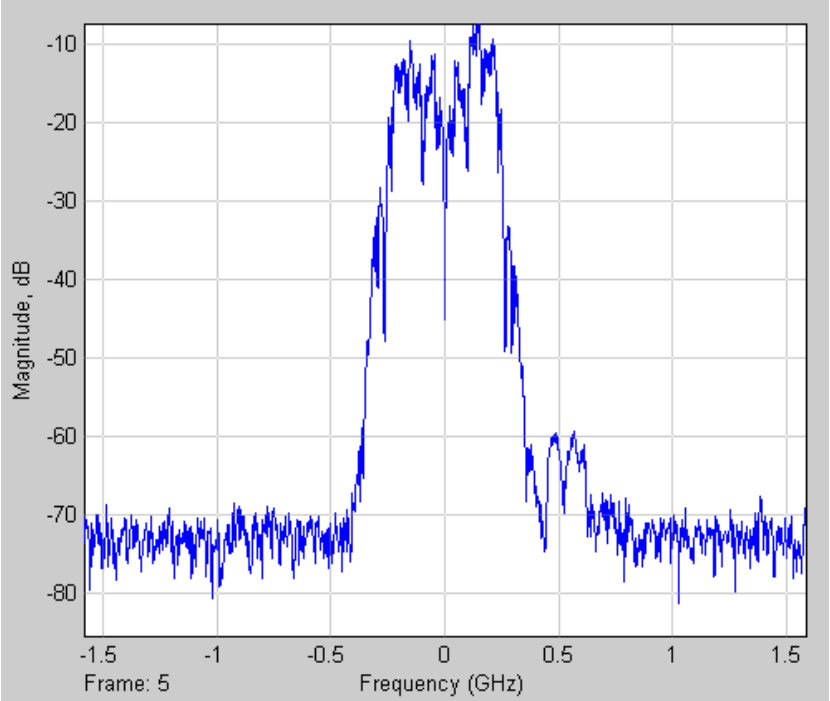

Figure 6-18 Baseband Original UWB Spectrum Before Clipping

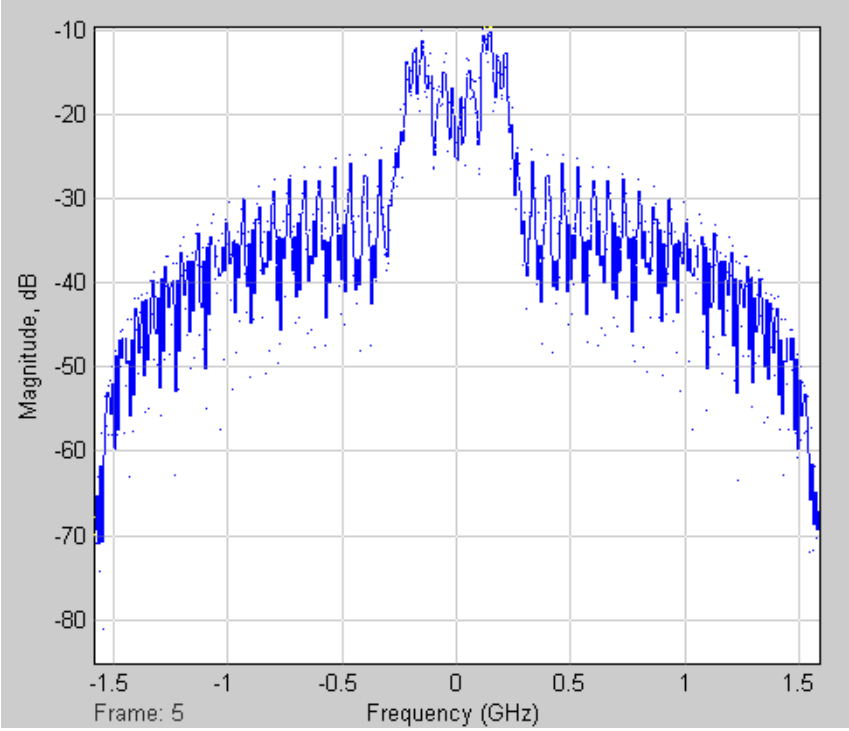

Figure 6-19 Baseband UWB Spectrum + Clipping

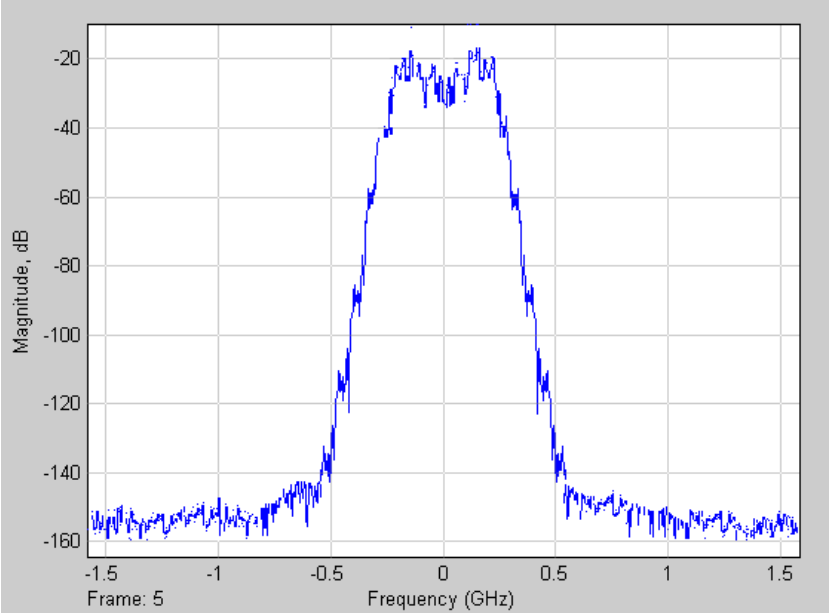

Figure 6-20 Baseband UWB Spectrum + Window-Clipping

To the best of our knowledge, this is a unique study that analysis and simulation are done on this pre-distortion technique to UWB OFDM signal to mitigate nonlinear effects of optical system.

6.2.3 Pre-distortion Method Analysis and Performance Simulation

Analysis and simulation is performed to evaluate the performance of the proposed signal pre-distortion methods in mitigating optical system non-linearity. From the previous discussion, we see that UWB OFDM signal with high dynamic range is very susceptible to nonlinear distortion. The proposed signal pre-distortion methods are designed to mitigate nonlinear effects of the optical system on the UWB OFDM signal in terms of reducing in-band and out-of-band noise due to nonlinear distortion. Because signal pre-distortion adds additional noise to the original signal, which diminishes the fruitfulness of signal pre-distortion process, there is a need to find a balance between nonlinear effects and the amount of signal pre-distortion to achieve best overall system performance. The object of the signal pre-distortion is to minimize combined noise due to

nonlinear distortion and signal pre-distortion. Shown in equation 6.7, $\widetilde{S}_t$ is the resulting signal after combined clipping and noise reduction process.

$$\widetilde{S}_t = S_t + C_t^{In} + C_t^{Out} + N_t^{In} + N_t^{Out} \tag{6.7}$$

where S_t is the original signal, C_t^{In} is the in band noise due to signal pre-distortion, C_t^{Out} is the out of band noise due to signal pre-distortion, N_t^{In} is in band noise due to nonlinear distortion, , N_t^{Out} is out of band noise due to nonlinear distortion.

The complex envelope of baseband OFDM signal and clipped signal from the simulation are shown in Figure 6-14 are Figure 6-15 respectively.

6.2.3.1.1 Out of Band Power

The out-of-band noise is the result of signal pre-distortion and nonlinear distortion. Equation 6.7 shows that out-of-band noise is generated both due to nonlinear distortion N_t^{Out} and signal Pre-distortion C_t^{Out}.

Firstly we evaluate out-of band noise due to the signal pre-distortion C_t^{Out}. One UWB channel occupies 528 MHz bandwidth. The signal pre-distortion operation generates a considerable amount of out of band noise across the RF carrier. However, window-clipping decreases the out-of-band pre-distortion noise C_t^{Out} by more than 40dB over the 528 MHz bandwidth. It is shown in Figure 6-20. This reduces cross talk between adjacent UWB channels. Secondly we evaluate out-of-band noise due to nonlinear distortion N_t^{Out}. With the increase in RF power to the electro-optic modulator, odd order RF harmonics power also increases. This severely affects system performance if the overall bandwidth is more than one octave. The proposed window-clipping reduces the out of band nonlinear distortion noise N_t^{Out} significantly which shown in Figure 6-21 and Figure 6-22.

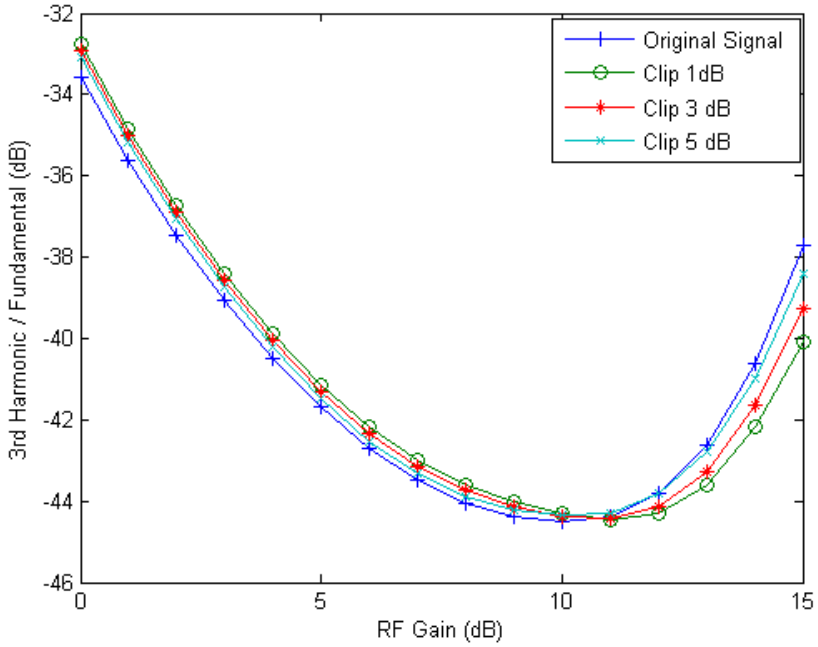

Figure 6-21 Third Harmonic to Fundamental Power vs. RF Gain

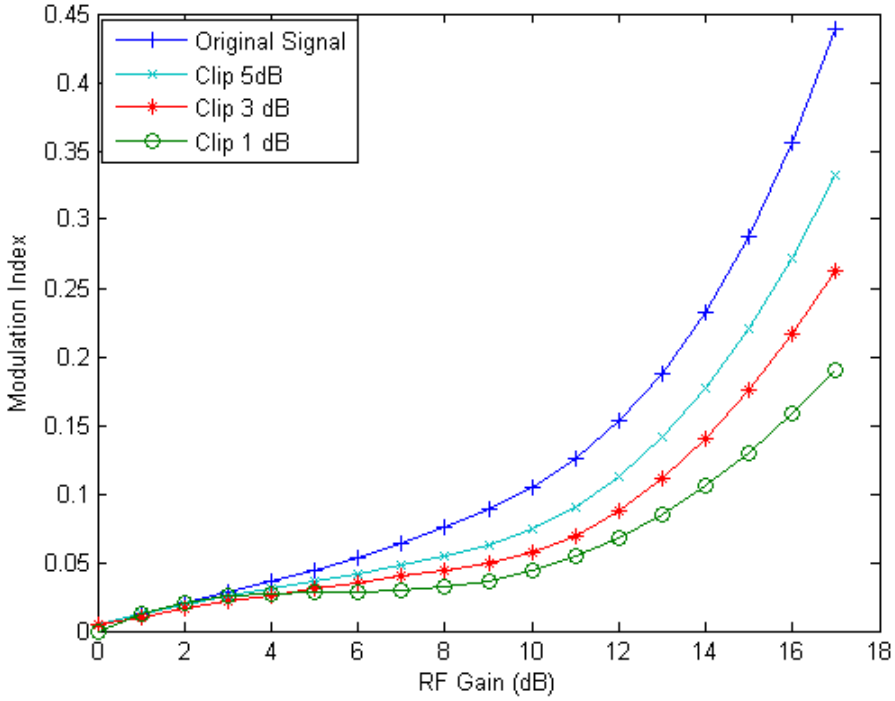

Figure 6-22 Modulation Index vs. RF Gain

Figure 6-21 and Figure 6-22 show that with the proposed signal pre-distortion method, the third harmonic RF power reduces by 3 - 4dB compared to the original signal when the modulation index is greater than 0.1. The reduction of RF power varies depending upon clipping threshold. From the analysis and simulation result, we can conclude that the proposed signal pre-distortion method reduces both out-of-band clipping noise and out of band nonlinear distortion noise.

6.2.3.1.2 Dynamic Range

Radio on Fiber system is comprised of many nonlinear devices such as electro-optic modulator, RF high power amplifiers, optical amplifiers, photo detector etc. With lower dynamic range of the pre-distorted signal, the RoF system has better performance against the combined nonlinear distortion of all of these nonlinear devices.

In previous section we discussed the susceptibility of the high peak to average power ratio (PAPR) of the OFDM signal makes to nonlinear distortions. The proposed signal pre-distortion methods reduce dynamic range of the OFDM signal. Simulation result in Figure 6-23 shows that the pre-distorted signal has a lower dynamic range compared to the original signal. With the clipping threshold decreases, the dynamic range of the signal reduces. Beyond a certain limit clipping noise becomes unacceptable. We can also see that apart from reduction in PAPR due to signal pre-distortion, the variation in PAPR of the pre-distorted signal is much less compared to the original signal. This eliminates the sudden occurrence of high peaks. As discussed in earlier sections, only a few peaks possess high amplitude. The proposed signal pre-distortion reduced the occurrence of the high peaks. Pre-distorted signal is less affected by nonlinear distortion, because of the lower dynamic range.

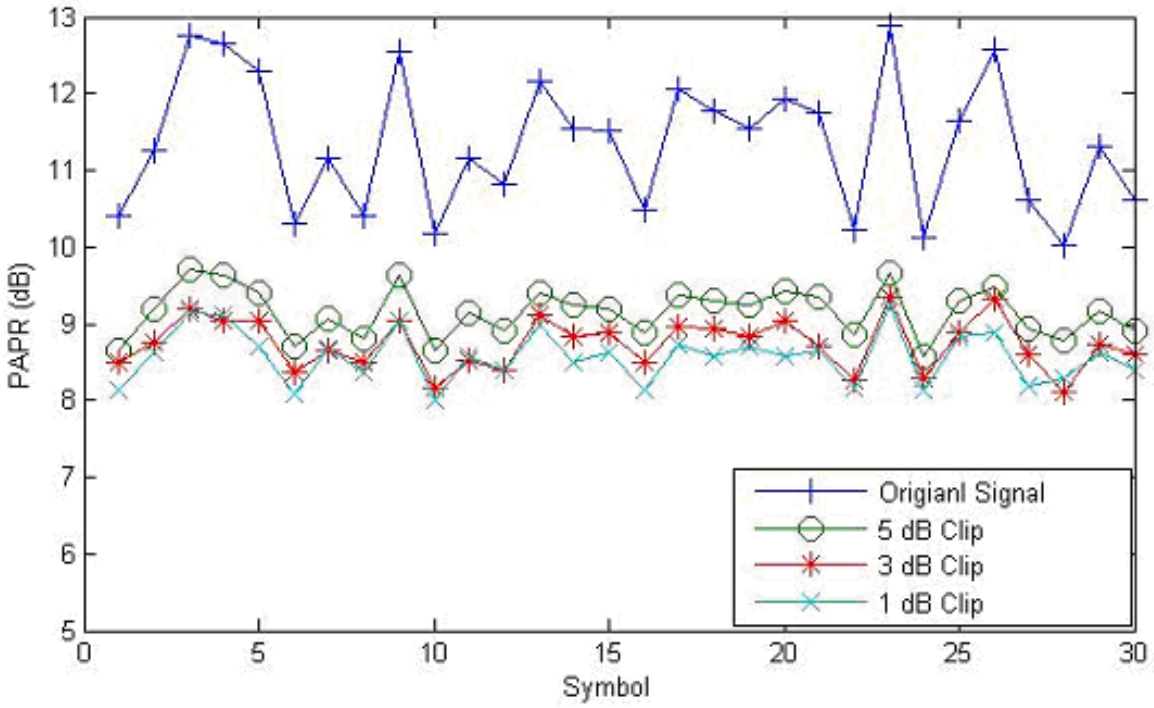

Figure 6-23 Peak to Average Power Ratio for Different Clipping Threshold

6.2.3.1.3 Constellation Error and Bit Error Performance

The bit error rate performance of the system depends on signal to in band noise ratio. Here, noise is comprised of noise due to nonlinear distortion, noise due to signal pre-distortion and additive noise. Nonlinear distortion noise and signal pre-distortion noise are interrelated. As clipping level increases nonlinear distortion reduces but clipping noise increases.

Figure 6-24 shows the RMS constellation error of the original signal, the baseband over sampled clipped signal and the window-clipped signal. The clipping threshold is 3, window function is Kaiser-3.6, SNR is 30 dB, and data rate is 480 Mbps. The original signal performs better than both signal pre-distortion methods below certain modulation index. In low modulation index region, in band nonlinear distortion noise is low and subsequently signal pre-distortion process in this region is not necessary. Pre-distortion only adds clipping noise without improving nonlinear distortion performance. But, when the modulation index increases to greater than a limit, increase in band nonlinear distortion noise surpasses in-band signal pre-

distortion noise and the window-clipped signal performs better in that region and the performance of pre-distorted signal becomes comparable to the original signal.

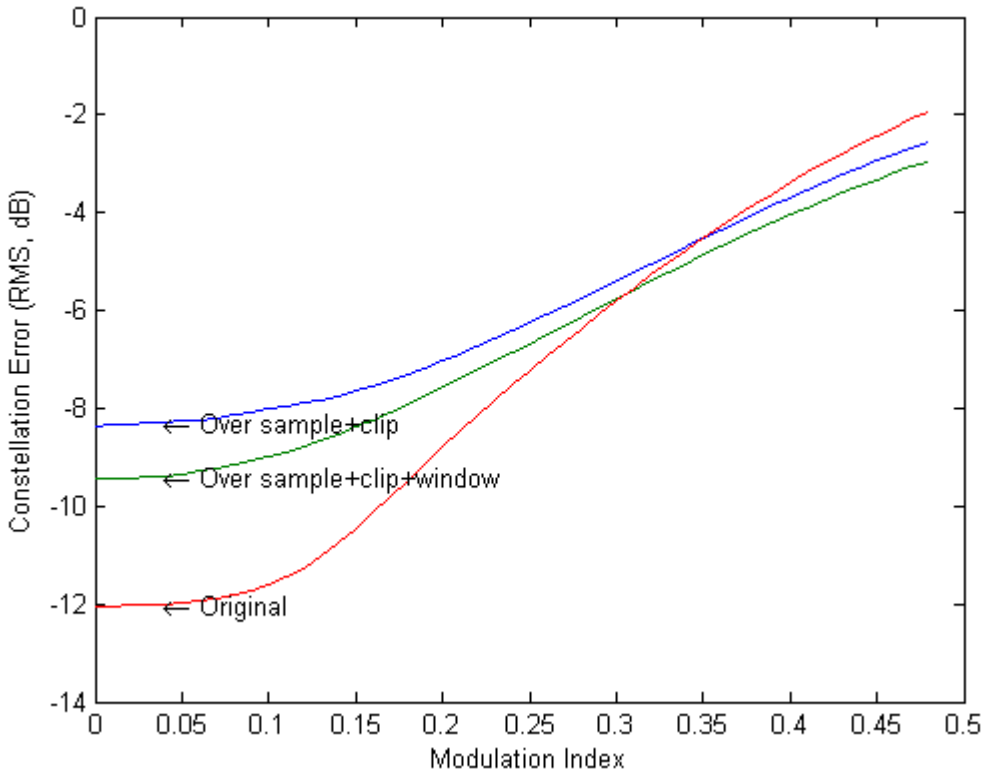

Figure 6-24 RMS Constellation Error vs. Modulation Index for Original Signal, Over Sampled + Clipped and Window-clipped Signal

In band noise caused by clipping degrades the bit-error-rate (BER) performance of the electric communication system. Figure 6-25 shows the BER performance as a function of signal-to-noise ratio (SNR) for the original signal, the baseband over sampled clipped signal and the window-clipped signal. The clip threshold is 3 dB, window function is Kaiser-3.6, modulation index is 0.35, and data rate is 480 Mbps. The modulation index for this test is 0.35, which is in the region in band nonlinear distortion noise surpasses in-band signal pre-distortion noise. We can see that both signals with pre-distortion perform better than the original signal. Signal with window-clipped distortion performs better than the over sampled clipped signal.

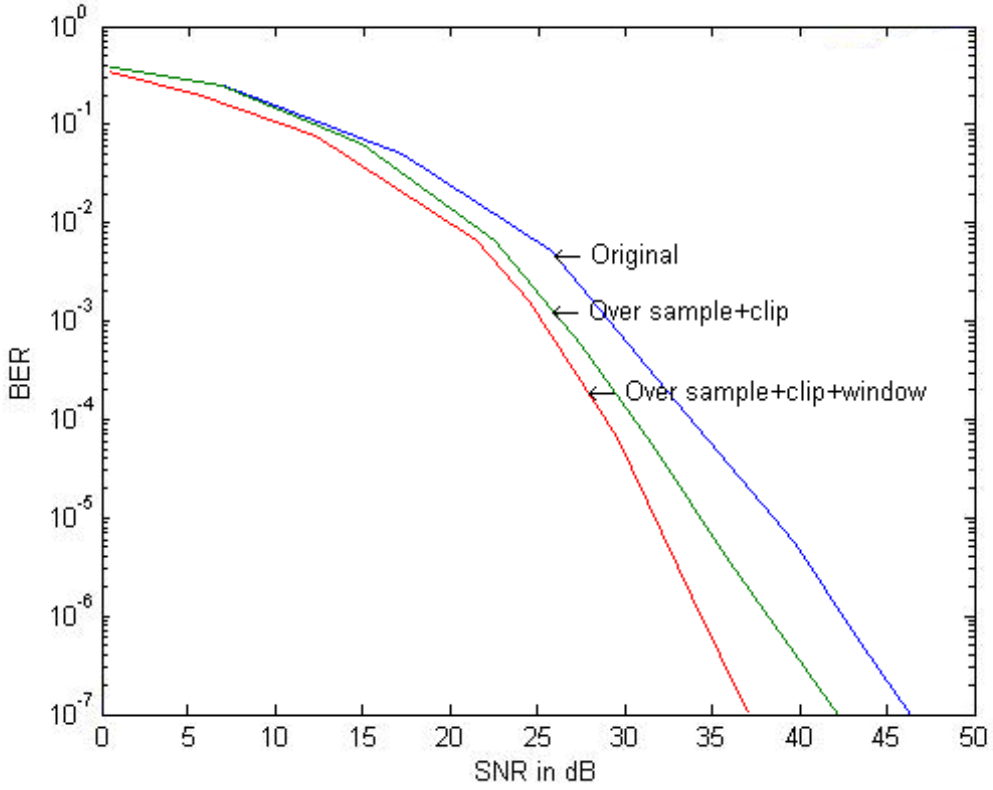

Figure 6-25 BER vs. SNR for Original Signal, Over Sampled + Clipped and Over Sampled + Clipped + Windowed Signal

6.2.4 Summary of UWB System

Pre-distortion is introduced to mitigate no-linear effect of optical system on UWB signal. The pre-distortion clipping including clipping threshold of 3, signal over sampling, and Kaiser 3.6 windowing is found to have the smallest constellation error.

The equalization step is to remove the effect of fiber dispersion and also any phase distortion due to electrical components. This is achieved by training the system with a known sequence, then comparing the phases of all received symbols with the transmitted symbols. The difference is recorded in a training file and shows a quadratic dependence with sub-carrier frequency, as expected from fiber dispersion.

6.3 UWB RoF Integration Simulation

With the result from optical and UWB system design and simulation, RoF system integration simulation is carried out. Integration test using both Roft Optisim and Matlab Simulink interconnected by implemented software connector. UWB signal with pre-distortion is generated and transmitted through single and multi mode VCSEL optical system. UWB RF signal in time domain is shown in Figure 6-26.

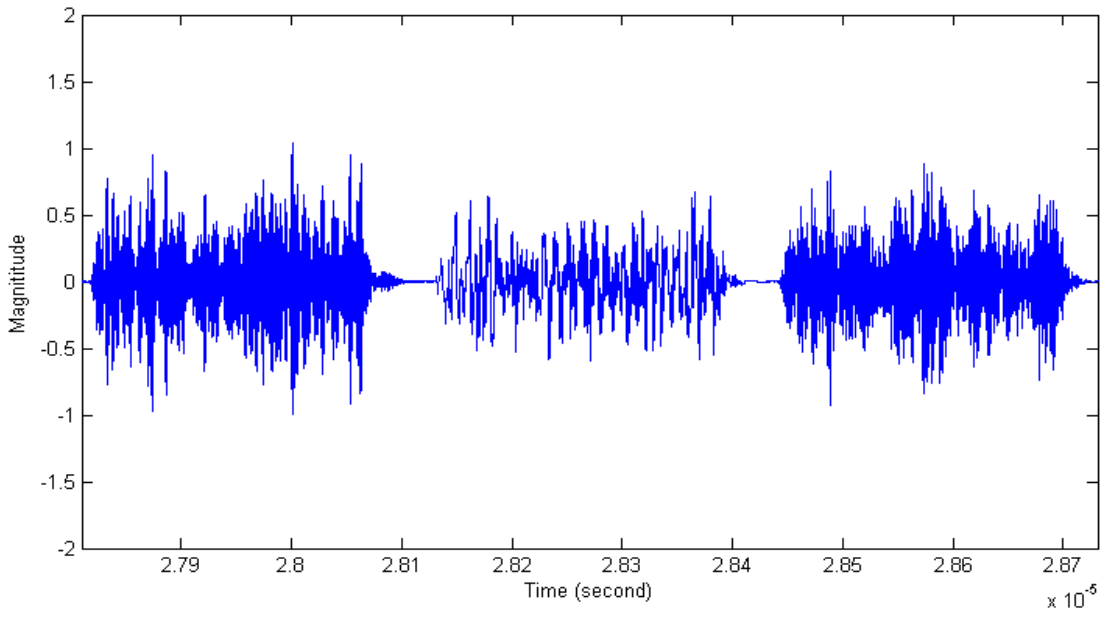

Figure 6-26 UWB RF Packet

Optical signal of single/multi mode VCSEL before launch to fiber and after received by PIN is shown in Figure 6-27 and Figure 6-28. Due the higher dispersion, multimode VCSEL shows about 10 dB lower in optical power after 0.5 km multimode fiber transmission. While single mode VCSEL does lose much optical power after the same fiber length.

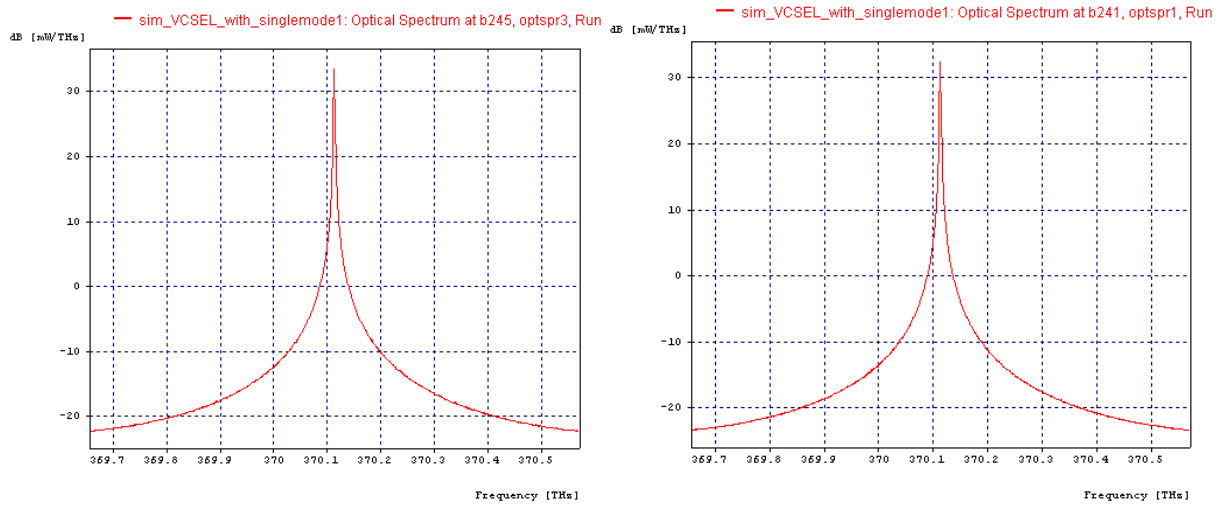

a) Before Transmission **b) After Transmission**

Figure 6-27 Single mode VCSEL optical spectrum

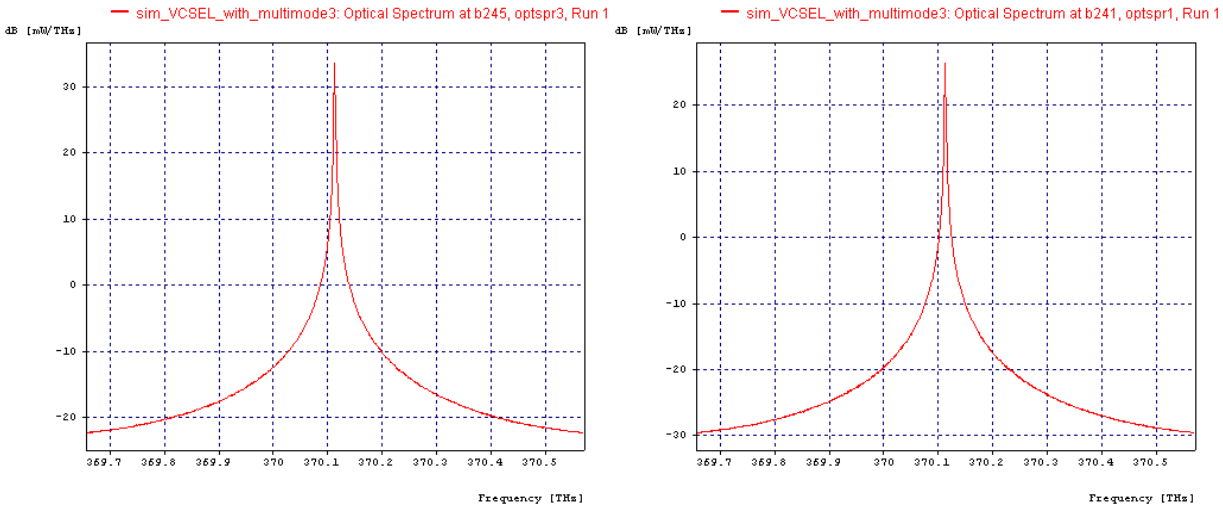

a) Before Transmission **b) After Transmission**

Figure 6-28 Multimode VCSEL Optical Spectrum

UWB RF signal in frequency domain before and after transmitted through single/multi mode optical system is shown in Figure 6-27 and Figure 6-28. UWB RF signal spectrum after optical transmission of multimode VCSEL is about 10 dB lower than that of single mode.

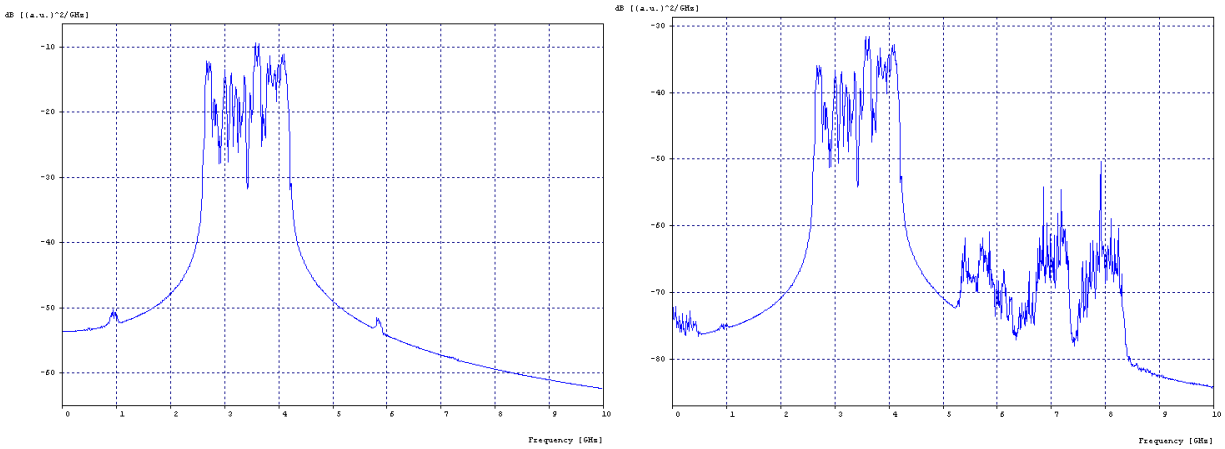

a) UWB Signal Before Single Mode VCSELb) UWB Signal After Single Mode VCSEL

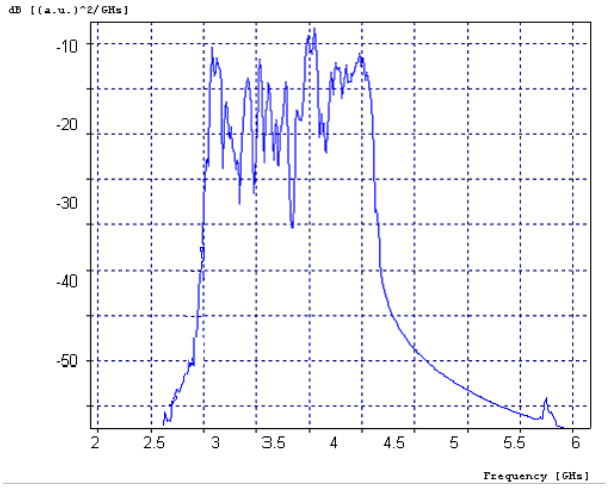

c) UWB Signal Before Multimode VCSEL c) UWB Single After Multimode VCSEL

Figure 6-29 UWB Electrical Spectrum

UWB QPSK eye diagram of single and multi mode VCSEL is shown in Figure 6-30. Single mode VCSEL has bigger eye opening that multimode VCSEL.

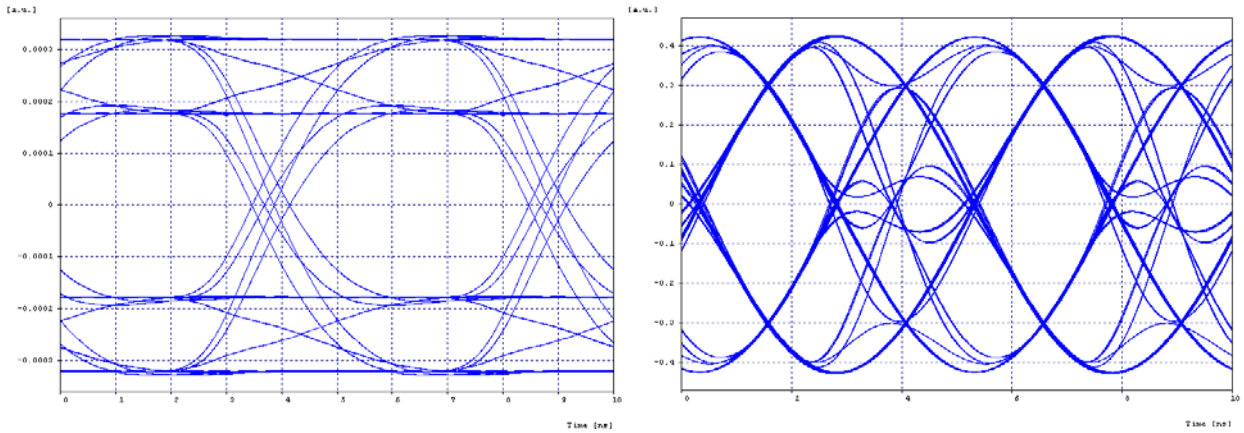

a) Single VCSEL and Fiber b) Multimode VCSEL and Fiber

Figure 6-30 In-phase Eye Diagram

Equalization of UWB QPSK signal removes the effect of fiber dispersion and also any phase distortion due to electrical components. Scattering diagram of UWB QPSK signal before and after equalization is shown in Figure 6-31.

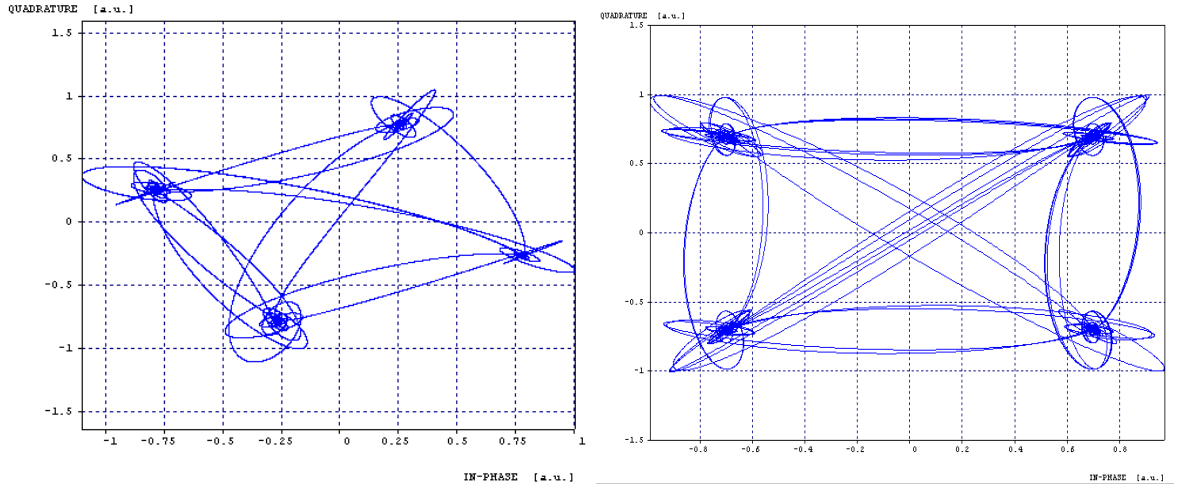

a) Before Equalization b) After Equalization

Figure 6-31 Quadrature Scattering Diagram

Digital data after RoF transmission is compared with the original digital data. The UWB data rate is at 480 Mbps. The BER at SNR 30 dB for single mode VCSEL RoF is 1.54302e-4. The BER at SNR 30 dB for multi mode VCSEL RoF is 3.4553e-4.

Chapter 7 Conclusion and Future Work

7.1 Thesis Summary and Conclusion

This thesis studies Radio on Fiber communication system using cost-effective VCSEL direct modulation to distribute UWB signal. The thesis is composed of four main sections. The first section (Chapter 1, 0 and Chapter 3) introduces radio-over-fiber (RoF) and ultra wide band (UWB) technologies. The second section (Chapter 4) studies properties of the components that form optical system of single and multi mode VCSEL. The third section (Chapter 5) studies non-linearity effect of OFDM from optical system. Pre-distortion method is proposed to mitigate high pick to average power (PAPR). The fourth section (Chapter 6) implements and simulates wireless and optical sub system of RoF based on the analysis from Chapter 4 and Chapter 5. Integration of wireless and optical simulation is carried out.

The behavior of UWB OFDM RF system and VCSEL optical system were analyzed theoretically and experimentally. An UWB OFDM signal pre-distortion method has been proposed to mitigate non-linear distortions for VCSEL RoF system. The pre-distortion method makes the UWB suitable for the transmission over VCSEL optical system. Various system configurations including signal mode and multi mode fiber have been considered. System simulation with commercial design and simulation software were performed. The performance of signal and multi mode VCSELs with various configurations is compared. Limitations are identified to optimize RoF system design. It is found that with proposed pre-distortion, optimized single mode VCSEL, for 500m optical link, SFDR of 80 – 90 dB $Hz^{2/3}$, the RoF system has the highest performance of 1.54302e-4 for the BER at SNR 30 dB, data rate 480 Mbps. The results show that low cost RoF system with optimized single mode VCSEL and pre-distortion method satisfies the requirements to distribute UWB RF signal.

7.2 Future Work

The UWB RoF system proposed in this thesis need to be validated in experiments. The off-the-shelf optical components referred in section 6.1.1 this thesis can be used for these experiments.

The properties of multimode VCSEL and method to mitigate the non-linearity need to be further studies to increase the performance of multimode VCSEL system.

Bibliography

[1] L. Yang and G.B. Giannakis, “Ultra Wideband communications,” IEEE Signal Processing Nov.2004.

[2] K. Siwiak, “UWB Propagation notes to P802.15 SG3a,” IEEE 802.15-02/328r0, July 2002.

[3] A.M. Saleh, A.J. Rustakoand R.S. Roman, “Distributed Antennas for indoor radio communications,” IEEE Trans. Commun. Vol. COM-35,np12 Dec 1987.

[4] D. Wake. Radio over Fiber Systems for Mobile Applications. In: Radio over Fiber Technologies for Mobile Communications Networks. Ed.: H. Al-Raweshidy, S. Komaki. Artech, Boston, pp.217-241, 2002.

[5] H. Bong Kim and A. Wolisz, “A radio over fiber based wireless access network architecture for rural area,” 14th IST Mobile and Wireless Commun. Summit, Dresden, June 2005.

[6] H. Al-Raweshidy and S. Komaki (ed.), Radio over Fiber Technologies for Mobile Communications Networks, Artech House 2002.

[7] Y. Watanabe, “Current Status of Perfluorinated GI-POF and 2.5 Gbps Data Transmission over it”, in Proceedings of OFC ‘03, USA, 2003, pp. 12 - 13.

[8] ITU, “World Telecommunication Development Report 2002: Reinventing Telecoms”, March, 2002.

[9] Y. Watanabe, “Current Status of Perfluorinated GI-POF and 2.5 Gbps Data Transmission over it”, in Proceedings of OFC ‘03, USA, 2003, pp. 12 - 13.

[10] D. K. Mynbaev, L. L. Scheiner, “Fiber Optic Communications Technology”, (Prentice Hall, New Jersey, 2001).

[11] J. Capmany, B. Ortega, D. Pastor, and S. Sales, “Discrete-Time Optical Processing of Microwave Signals”, JLT, Vol. 23, No. 2, 703 - 723, (2005).

[12] D. Wake, S. Dupont, C. Lethien, J-P. Vilcot, and D. Decoster, “Radiofrequency Transmission over Multimode Fiber for Distributed Antenna System Applications”, Electronic Letters, Vol. 37, No. 17, pp 1087 - 1089 (2001).

[13] M. Bass, E. W. Stryland, “Fiber Optics Handbook”, McGraw_hill, 0-07-138623-8

[14] J. J. O’Reilly, P. M. Lane, and M. H. Capstick , “Optical Generation and Delivery of Modulated mm-waves for Mobile Communications”, in Analogue Optical Fibre

Communications, B. Wilson, Z. Ghassemlooy, and I. Darwazeh, ed. (The Institute of Electrical Engineers, London, 1995).
[15] D. Novak, "Fiber Optics in Wireless Applications", OFC 2004 Short Course 217, 2004.
[16] M. Varasi. Fast Modulators. In: Microwave Photonics. Ed. By A.Vilcot, B. Cabon, J. Chazelas. Kluwer, Boston, pp. 57-73, 2003.
[17] Peters F H and MacDougal M H 2001 IEEE Photon. Technol. Lett. 13 645.
[18] Van Nee, R.; de Wild, A.; "Reducing The Peak-To-Average Power Ratio of OFDM", Vehicular Technology Conference, 1998. VTC 98. 48th IEEE, Volume:3, 18-21 May 1998, pages: 2072-2076 vol. 3
[19] Davide Dardari, Velio Tralli, and Alessandro Vaccari; "A Theoretical Characterization of Nonlinear Distortion Effectis in OFDM Systems", IEEE Transactions On Communications, Vol. 48, No. 10, October, 2000
[20] C. Minot, "Electroabsoprtion Modulators and Photo-Oscillators for conversion of Optics to Millimeter waves", In: Microwave Photonics. Ed. By A. Vilcot, B. Cabon, J. Chazelas. Kluwer, Boston, pp. 73-81, 2003.
[21] Cox CIII, Ackerman E, Helkey R and Betts G E 1997 IEEE Trans. Microwave Theory Technol. 45 1375
[22] K. Petermann, Laser Diode Modulation and Noise, Kluwer Academic Publishers, Dordrecht, 1988.
[23] C.K Sim, M.L. Yee, B. Luo, L.C. Ong, M.Y.W. Chia, "Performance evaluation for wireless LAN, Ethernet and UWB co-existence on hybrid Radio-over-Fiber Picocells," OFC/NFOEC JWA60 Conf. 2005.
[24] Simon Shepherd, John Orriss, and Stephen Barton; "Asymptotic Limits in Peak Envelope Power Reduction by Redundant Coding in Orthogonal Frequency-Division Multiplex Modulation", IEEE Transactions on Communications, Vol. 46, No. 1, January 1998.
[25] C. H. Cox, Analog optical links theory and Practice, Cambridge University press 2004.
[26] B. Allen (Ed.), "Ultra Wideband: Technology and future perspectives," WWRF White Paper V3.0 March 2005.
[27] Q. Shi, R. S. Burroughs, and D. Lewis, "An alternative model for laser clipping-induced nonlinear distortion for analog lightwave CATV systems," IEEE Photon Technol. Lett., **4** (7), 784–7, 1992.

[28] J. Kelly IEEE P802.15.3a Working Group for Wireless Personal Area Networks, "MB-OFDM Physical layer submission," IEEE 802.15- 04/0122r4, March 2004.
[29] Coldren L A and Corzine S W 1995 Diode Lasers and Photonic Integrated Circuits (New York: Wiley).
[30] Kjebon O, Schatz R, Lourdudoss S, Nilsson S and Stålnacke B 1996 SPIE Proc. 2684 138.
[31] R. V. Nee, R. Prasad, "OFDM for Wireless Multimedia Communications", Artech House, ISBN 0-89006-530-6.
[32] Xiaodong Li and Leonard J. Cimini, Jr.; "Effects of Clipping and Filtering on the Performance of OFDM", IEEE, 1997
[33] Denis J. G. Mestdagh, Paul Spruyt and Bernard Biran; "Analysis of Clipping Effect in DMT-based ADSL Systems", IEEE, 1994
[34] K. Kishino, "Direct modulation of semiconductor lasers," in Handbook of Semiconductor Lasers and Photonic Integrated Circuits, eds. Y. Suematsu and A. R. Adams, Chapman & Hall, London, 1994.
[35] Ahmad R. S. Bahai, Manoneet Singh, Andrea J. Goldsmith, and Burton R. Saltzberg; "A New Approach for Evaluating Clipping Distortion in Multicarrier Systems", IEEE Journal on Selected Areas in Communications, Vol. 20, No. 5, June 2002.
[36] Yang Jun, Yang Jiawei and Li Jiandong; "Reduction of the Peak-to-Average Power Ratio of the Multicarrier Signal via Artificial Signals", IEEE, 2000
[37] Ahmad R. S. Bahai, Manoneet Singh, Andrea J. Goldsmith, and Burton R. Saltzberg; "A New Approach for Evaluating Clipping Distortion in Multicarrier Systems", IEEE Journal on Selected Areas in Communications, Vol. 20, No. 5, June 2002.
[38] T. Yoshikawa, T. Kawakami, H. Saito, H. Kosaka, M. Kajita, K. Kurihara, Y. Sugimoto, and K. Kasahara, "Polarization-controlled single-mode VCSEL," IEEE J. Quantum Electron., **34** (6), 1009–15, 1998.
[39] H. Lee, R. V. Dalal, R. J. Ram, and K. D. Choquette, "Resonant distortion in vertical cavity surface emitting lasers for RF communication," Optical Fiber Conference
[40]Anuj Batra et al., "IEEE P802.15 Wireless Personal Area Networks", IEEE P802.15 Working Group for Wireless Personal Area Networks, 03 March, 2003
[41] D. K. Mynbaev, L. L. Scheiner, "Fiber Optic Communications Technology", (Prentice Hall, New Jersey, 2001)

[42] J. Piprek, K. Takiguchi, A. Black, P. Abraham, A. Keating, V. Kaman, S. Zhang, and J. E. Bowers, “Analog modulation of 1.55 μm vertical cavity lasers,” Proc. SPIE, 3627, Vertical-Cavity Surface-Emitting Lasers III, eds. K. D. Choquette and C. Lei, 1999.
[43] Robert James Davies, "Optical Single Sideband for Broadband and Subcarrier Systems", PhD Thesis, University of Alberta, Canada, 1999.
[44] Juha Heiskala, John Terry, “OFDM Wireless LANs: A Theoretical and Practical Guide”, Sams Publishing, ISBN: 0672321572, 2002.
[45] Gustavsson J S, Haglund Å, Carlsson C, Bengtsson J and Larsson A 2003 IEEE J. Quantum Electron. 39 941